

FACULTY OF TECHNOLOGY

NO_X EMISSION CONTROL OF EXHAUST GASES FROM AMMONIA ENGINE WITH VANADIUM AND IRON SCR CATALYSTS

Jaakko Petrelius

PROCESS ENGINEERING

Master's thesis

June 2026

ABSTRACT

NO_x emission control of exhaust gases from ammonia engine with vanadium and iron SCR catalysts

Jaakko Petrelius

University of Oulu, Degree Programme in Process Engineering

Master's thesis, 2026, 85 pp.

Supervisors at the university: Mika Huuhtanen Docent, D.Sc.(Tech.), Teuvo Maunula Prof. of Practice, D.Sc.(Tech.)

Tightening CO_2 legislations in the automotive and marine industry has sparked major discussions regarding alternative, carbon free fuels such as ammonia. Though ammonia is carbon free, a high amount of nitrogen oxides (NO_x) is released in combustion. The selective catalytic reduction by ammonia (NH_3-SCR) has been applied world-wide to decrease NO_x emissions.

It is important to investigate the ammonia adsorption-desorption phenomena on the SCR catalysts, to understand better the NH_3-SCR reactions. Using transient kinetic methods together with mass spectrometry, it is possible to detect and interpret adsorption and desorption rates and capacities.

Experiments were conducted at the Heterogenous catalysis laboratory at the Chemistry Department of the University of Cyprus. In this Master's thesis, extruded and coated vanadium (V) SCR and iron (Fe) SCR catalysts were investigated by transient kinetic methods under various conditions. The effect of water, N_2O and oxygen was investigated on SCR and platinum catalysts by NH_3 adsorption-desorption experiments at 150-400 ºC. The presence of water (5%) increased NH_3 adsorption on V-SCR but decreased on the Fe-SCR catalyst. 50 ppm N_2O present in reaction conditions decreased clearly NH_3 adsorption on the Fe-SCR but had a negligible effect on the V-SCR catalyst. These transient results showed the differences between NH_3-SCR catalysts in exhaust conditions and were applied to evaluate the existing theories for NH_3 adsorption.

Keywords: Adsorption, ammonia, iron, mass spectrometry, SCR, transient kinetic, vanadium

TIIVISTELMÄ

NO_x päästöjen hallinta ammoniakkimoottorin pakokaasuista vanadiini- ja rauta-SCR katalyyteilla

Jaakko Petrelius

Oulun yliopisto, Prosessitekniikan tutkinto-ohjelma

Diplomityö, 2026, 85 s.

Työn ohjaaja / ohjaajat yliopistolla: Mika Huuhtanen Dosentti TkT, Teuvo Maunula työelämäprofessori, TkT.

Tiukentunut lainsäädäntä auto- ja meriteollisuuden CO_2 päästöjen suhteen on herättänyt paljon keskustelua vaihtoehtoisista, hiilivapaista polttoaineista kuten ammoniakista. Vaikka ammoniakki on hiilivapaata, sen palamisessa vapautuu suuria määriä typen oksideja (NO_x). Selektiivistä katalyyttistä pelkistystä ammoniakilla (NH_3-SCR) on käytetty maailmanlaajuisesti NO_x-päästöjen vähentämiseksi.

On tärkeää tutkia ammoniakin adsorptio-desorptioilmiöitä SCR-katalyyteillä, jotta NH_3-SCR-reaktioita ymmärrettäisiin paremmin. Käyttämällä transienttikinetiikan menetelmiä massaspektrometrian avulla voidaan mitata ja analysoida ammoniakin adsorptio- ja desorptionopeuksia sekä -määriä erilaisissa olosuhteissa.

Mittaukset tehtiin Kyproksen yliopiston kemian laitoksessa heterogeenisen katalyysin laboratoriossa. Tässä opinnäytetyössä tutkittiin ammoniakin reaktioita vanadiini (V)- ja rauta (Fe)-SCR-katalyyteissä transienttikineettisten menetelmien avulla. Veden, N_2O:n ja hapen vaikutusta tutkittiin NH_3:n adsorptio- desorptioon SCR- ja platinakatalyyteillä 150–400 ºC. Veden läsnäolo (5%) nosti hieman NH_3-adorptiokapasiteettiä V-SCR-katalyyteillä, mutta heikensi Fe-SCR-katalyyteillä. N_2O (50 ppm) seoksessa vähensi selvästi NH_3:n adsorptiota Fe-SCR-katalyyttiin, mutta sillä oli vähäinen vaikutus V-SCR-katalyytin adsorptioon mittausolosuhteissa. Nämä transienttikokeet näyttivät erot SCR-katalyyttien välillä pakokaasuolosuhteissa ja niitä sovellettiin NH_3-adsorptioteorioden arviointiin

Asiasanat: Adsorptio, ammoniakki, massaspektrometria, rauta, SCR, transienttikinetiikka, vanadiini

PREFACE

This work was conducted as a part of the Flex-CPT project co-funded by Business Finland. I graciously acknowledge the financial support received for this thesis by the project and its funding partners.

I am profoundly grateful for the support and guidance of my supervisors Docent Mika Huuhtanen and Professor of practice Teuvo Maunula. My sincerest thanks to Mika for welcoming me into the project and offering valuable guidance and expertise during the project. I would also like to express my thanks to Teuvo for his expertise in the field of emission control technologies as well as his support throughout the project. It was a pleasure working with you both on this project. I would also like to thank the ECE research group for providing a productive and comfortable working environment.

I would like to sincerely thank Professor (em.) Angelos M. Efstathiou for providing me with the opportunity to conduct the experiments at the University of Cyprus. I am particularly grateful for your invaluable expertise, guidance and support in transient kinetics and catalysis research which were instrumental in the completion of this study.

I am also deeply grateful to doctoral student Georgia-Maria Zarkou for her effort, guidance and valuable assistance throughout this project during my stay in Cyprus. I hope your future work continues to reflect the same enthusiasm and positivity that made my stay both memorable and pleasant.

Finally, I would like to thank my friends and family for all the support I have received during my time studying. I am fortunate to be surrounded by such remarkable people as you.

Oulu 9.6.2026

Jaakko Petrelius

TABLE OF CONTENTS

ABSTRACT
TIIVISTELMÄ
PREFACE
TABLE OF CONTENTS
ABBREVIATIONS
SYMBOLS 8
1 INTRODUCTION 9
2 AMMONIA 11
2.1 Green ammonia synthesis 12
2.2 Ammonia as fuel 14
3 SELECTIVE CATALYTIC REDUCTION 16
3.1 Reaction network 16
3.2 NH_3-SCR catalysts 17
3.2.1 Zeolite-based iron and copper catalysts 17
3.2.2 Vanadium-based catalysts 18
3.2.3 NH_3-SCR catalysts structure 20
3.3 NH_3-SCR applications 21
3.3.1 Stationary and marine applications 22
3.3.2 Mobile SCR application – vehicles and nonroad machinery 25
4 AMMONIA ADSORPTION AND OXIDATION 27
4.1 Ammonia adsorption 27
4.1.1 Lewis and Bronsted acid adsorption sites 27
4.1.2 Transient adsorption studies on vanadium-based catalysts 29
4.1.3 Transient adsorption studies on iron-based catalysts 29
4.1.4 Moisture effect on NH_3 adsorption 31
4.2 Ammonia oxidation reaction 32
5 EXPERIMENTAL 34
5.1 Catalysts 34
5.2 Texture characterization of catalysts 34
5.3 Transient kinetic experiments setup 35
5.3.1 Gas flow and reactor system 35
5.3.2 Mass spectrometry gas analysis 37

5.4 Transient kinetic experiments 37
5.4.1 Ammonia adsorption/desorption on NH_3-SCR catalysts in dry conditions (TE1) 37
5.4.2 Effect of N_2O on ammonia adsorption (TE2) 39
5.4.3 Ammonia adsorption-oxidation in dry conditions (TE3) 39
5.4.4 Ammonia adsorption on SCR catalysts in wet conditions (TE4) 39
5.4.5 Mass spectrometry analysis 40
6 EXPERIMENTAL RESULTS 42
6.1 Catalysts characterization 42
6.2 Ammonia adsorption on SCR catalysts in dry conditions 42
6.2.1 Effect of temperature 42
6.2.2 Effect of ammonia concentration 50
6.2.3 Effect of catalyst composition 60
6.3 Effect of N_2O on ammonia adsorption/desorption 62
6.4 Ammonia adsorption followed by oxidation (dry conditions) 66
6.5 Ammonia adsorption on SCR catalysts in wet conditions 70
7 SUMMARY OF RESULTS 75
8 CONCLUSIONS 77
REFERENCES

ABBREVIATIONS

AH	Air Heater
Ar	Argon
ASC	Ammonia slip catalyst
ATS	Aftertreatment system
BET	Brunauer-Emmet-Teller
DOC	Diesel oxidation catalyst
DPF	Diesel particulate filter
ESP	Electrostatic precipitator
Fe-SCR	Iron-SCR catalyst
Fe_xO_y	Iron oxides
FGD	Flue gas desulfurizer
GHG	Greenhouse gas
GHSV	Gas Hourly Space Velocity
HC	Hydrocarbon
H-ESP	Hot side electrostatic precipitator
HP-SCR	High-performance SCR
LP-SCR	Low-performance SCR
N2	Nitrogen gas
N_2O	Nitrous oxide
NH_3	Ammonia
NH_3-SCR	Ammonia SCR
NO_x	Nitrogen oxides
PEM	Polymer exchange membrane electrolysis
PID	Proportional-Integral-Derivative
PM	Particulate matter
Pt	Platinum
Pt-DOC	Platinum diesel oxidation catalyst
RDS	Rate-determining step
SCR	Selective catalytic reduction
SO_2	Sulphur dioxide
SOEC	Solid oxide electrolysis
TPD	Temperature programmed desorption
V-SCR	Vanadium SCR catalyst

SYMBOLS

I_x^{Sens}	Signal of calibration gas
F	Total molecular flow (mol/s)
$F_{x(t)}$	Molar flow rate (mol/s)
I	Raw signal
I^{bck}	Background signal
I^{bp}	Gas signal in feed gas stream
R_ads	Rate of adsorption
R_des	Rate of desorption
w	Catalyst mass
y_x	Mole fraction of adsorption gas
$Z_{i(t)}$	Dimensionless signal in relation to time(s)
$Z_{Kr(t)}$	Dimensionless concentration of krypton tracer gas
$Z_{x(t)}$	Signal of adsorption gas in relation to time

1 INTRODUCTION

Upcoming industrial legislations regarding CO_2 emission limits has sparked major upheaval in the industry. European union has set ambitious emissions standards for the automotive industry for 2035, demanding zero grams of CO_2 emissions for vehicles Similarly, shipping industry makes up a large portion of world trade, which is expected to rise in the future. (Egerer et al., 2023) Concerns regarding marine exhaust have sparked debate over the years, which has led to an increasing attention regarding their potential long-term negative effects on the environment and health. Marine fuels are generally considered to be less clean due to their usage in large engines, especially regarding sulphur content. Marine exhaust gases make up a large portion of the global CO_2, NO_x, SO_2 and particulate matter (PM) emissions. (Zannis et al., 2022; Lehtoranta et al., 2015) Due to tightening emission regulations, new alternative fuels are being considered for both automobile and marine industry to reach these targets.

Ammonia as an alternative to carbon-based fuels has been proposed as an energy source for achieving carbon-free emission goals. It possesses several properties that make it an attractive replacement or addition to conventional fuels, particularly due to its carbon-free composition (no HCs, CO or particulate emissions). However, the use of ammonia as a fuel leads to the higher formation of nitrogen-containing compounds such as NO_x (from air and much less from fuel) and N_2O, which can be even more harmful by the greenhouse gas effect than carbon dioxide in terms of environmental impact. These harmful compounds cannot be released into the environment, thus requiring aftertreatment (Chen et al., 2024; Nova and Tronconi, 2014).

To reduce these harmful emissions, NO_x removal is required. Selective catalytic reduction (SCR) is a method in which NH_3 reacts with nitrogen oxides (NO_x) in the presence of a catalyst to produce nitrogen gas and water. NH_3-SCR catalytic technology is the main solution also for NO_x removal in NH_3 engine applications (Nova and Tronconi, 2014; Lehtoranta et al., 2015).

The SCR has been utilized for a long time in power plants and later in mobile and stationary NO_x control applications, where it has proven to be an effective method for reducing NO_x emissions. Over time, SCR catalysts have been continuously developed

and optimized for a wide range of applications, such as marine and on wheels applications improving their efficiency, durability, and suitability for different operating conditions. Depending on the operating conditions, such as exhaust composition, temperature and flow rate, different catalytic reactions can occur. The selectivity of the SCR reaction to the network varies depending on the composition of the catalyst (Nova and Tronconi, 2014).

The focus of this Master's thesis is to determine how different SCR and oxidation catalysts behave under different simulated exhaust gas conditions using transient kinetics monitored with on-line mass spectrometry. The experimental section of this thesis focuses on how extruded and coated vanadium (V)- and coated iron (Fe)-based catalysts, and a platinum (Pt) oxidation catalyst behave under ammonia exhaust gas environment (dry, wet, presence of oxygen and N_2O). The current and future ammonia production methods are reviewed along with basic mechanisms of SCR reactions, catalysts and system configurations used in different applications. Supporting the experiments in this research, similar studies reported in the literature were also reviewed and discussed.

2 AMMONIA

Ammonia NH_3 is a widely used chemical compound, especially in the manufacturing of fertilizers and as a precursor in the production of other chemicals. Ammonia is mainly synthesized by the Haber-Bosch process, in which ammonia is formed in the reaction between hydrogen (H_2) and nitrogen (N_2) at high temperature and pressure in the presence of an iron catalyst (Appl, 2011; Smart, 2022).

Industrial ammonia production can be roughly divided into three stages: Synthetic gas (N_2/H_2 gas mixture) production, compression of synthetic gas, and ammonia synthesis in the presence of a catalyst. In the synthetic gas production stage, the gas mixture containing hydrogen and nitrogen is prepared for the process. Hydrogen is produced and separated from syngas (CO/H_2 gas mixture) made through a catalytic steam reforming process utilizing desulphurized natural gas. Nitrogen is produced from the air (separation of N_2 from O_2) for the process (Appl, 2011; Smart, 2022).

Ammonia is mainly produced for the use in fertilizer industry, contributing over 83% of all the ammonia produced. Industrial ammonia is mostly used to produce nitric acid or other chemicals, such as sodium nitrate or ammonium chloride. Currently the amount of ammonia produced annually is ~176 million tonnes and the amount rises annually. Ammonia is also used environmentally for the reduction of SO_2 produced in fossil fuel power plants as well as in the selective catalytic reduction of NO_x in both stationary applications, such as power plants, and in mobile applications, such as diesel vehicles and ships (Appl, 2011).

2.1 Green ammonia synthesis

The advancements in green energy applications poses a big opportunity to utilize green energy in highly energy demanding industrial chemical processes, such as the Haber-Bosch, while making it a carbon-free process. (Smart, 2022). Because hydrogen is produced for Haber-Bosch process mainly by steam reforming of fossil natural gas, the current ammonia synthesis process creates a lot of carbon dioxide emissions, which could be credited for up to 1% of the total carbon dioxide emissions globally. Decarbonizing ammonia production process has been a major undertaking regarding global carbon dioxide emission goals. (Appl, 2011).

Methods regarding future NH_3 emission control can be divided into *blue* ammonia and *green* ammonia. Blue ammonia aims to reduce CO_2 emissions by utilizing carbon capture technology for the formed CO_2 in natural gas reforming process. Green ammonia process is focused on the use of alternative renewable energy raw materials (H_2, N_2) for the process. In the green ammonia production, hydrogen is produced through green, alternative methods such as electrolysis of water using sustainable electricity sources such as wind, solar, geothermal energy or from biomass utilization (Smart, 2022; Egerer et al., 2023).

Modern green energy applications for the Haber-Bosch process mainly focus on hydrogen production by replacing natural gas (source material). Water electrolysis in general is known as a strong candidate for hydrogen production, but other methods are still under development as contenders, such as the electro- and photochemical synthesis. (Smart, 2022; Egerer et al., 2023). Alternatively, Haber-Bosch process could be replaced entirely by a direct synthesis of hydrogen and nitrogen either through renewable electrochemical or photochemical methods (Smart, 2022).

Prominent electrolyser technologies include alkaline, PEM (proton exchange membrane) and SOEC (solid oxide electrocatalyst) electrolyses. PEM and solid oxide methods are still under development but show potential for higher efficiency in the future when compared with conventional electrolysis. Alkaline electrolysis is a well-established

method for modern hydrogen production, having a high energy efficiency with high hydrogen purity yield. (Smart, 2022; Carmo et al., 2013).

In alkaline electrolysis two electrodes are submerged in a liquid alkaline electrolyte that consists either of sodium hydroxide (NaOH) or potassium hydroxide (KOH) solutions. The electrodes are separated from each other by a diaphragm to allow produced gases to separate (Carmo et al., 2013). Currently both PEM and SOEC electrolyses are commercially expensive (Smart, 2022; Carmo et al., 2013). PEM is more considered as an alternative electrolysis method, which differs from alkaline electrolysis by utilizing a polystyrene membrane as an electrolyte. The thin membrane allows for a compact, high proton conducting system that can be utilized in higher pressures when compared to alkaline electrolysis. The membrane allows for a higher energy efficiency when compared with conventional electrolysis, while similarly compressing gas in higher pressure, which reduces costs. Electrolysis based on SOECs utilizes fuel cells technology for hydrogen production. The SOEC is seen as an alternative due to high potential efficiency with low requirements regarding operating environment, but currently it is still under development (Smart, 2022; Carmo et al., 2013).

Other experimental methods include electrochemical synthesis of hydrogen as well as photochemical synthesis of ammonia. In the electrochemical synthesis, hydrogen and nitrogen are directly synthesized into ammonia through renewable energy sources. This method is currently not yet feasible due to efficiency issues regarding high energy requirements, catalyst conversion as well as selectivity weakness. Photochemical synthesis uses sunlight to produce ammonia directly from nitrogen and hydrogen via photocatalysis. The photocatalyst operates as a semiconductor that absorbs solar energy, after which it activates the semiconductor with the consequence to excite electrons for facilitating nitrogen and hydrogen chemisorption and surface chemical steps towards ammonia formation. Photocatalysts are currently lacking in their catalytic activity, being roughly 1000 times less active than their thermo/electrochemical counterparts (Smart, 2022).

The main inhibiting factor for utilizing green energy for hydrogen production is the high energy loss. (Smart, 2022; Carmo et al., 2013). Main contributing factor is the energy

required for the electrolysis process, which attributes as the major energy consumption, whereas other factors include the need of water for the electrolysis process, which limits applications in low water content environments (Smart, 2022).

2.2 Ammonia as fuel

Ammonia is promising as a fuel for its high energy density, being carbon and sulphur free, being easy to store, as well as being excellent hydrogen storage medium. Main emissions include NO_x and N_2O as the result of combustion of NH_3 in air (thermal-NO_x from air-N_2 and fuel-NO_x from NH_3) but also unburned ammonia is released (NH_3-slip) (Smart, 2022; Chen et al., 2024).

Ammonia is usually stored in liquid form, either through pressure, atmospheric or a reduced pressure storing. The pressure and atmospheric ones are the most used methods. (Appl, 2011). Ammonia storing is relatively easier due to stable conditions than storing hydrogen or other hydrogen carriers such as propane. (Appl, 2011; Reiter and Kong, 2011). Ammonia liquefies at moderate pressures corresponding to ca. -33 ºC and has a high hydrogen density of 17.8 wt%, which makes ammonia a good hydrogen carrier from logistical and safety viewpoint (Appl, 2011)

Transporting ammonia is thus also easier and safer when compared to other hydrogen carriers such as methane or propane. (Appl, 2011; Reiter and Kong, 2011) When compared with the current hydrogen production and shipping infrastructure, the infrastructure of ammonia production and shipping is already mature for a growing demand annually. (Appl, 2011; Reiter and Kong, 2011; Egerer et al., 2023) Large-scale production of green hydrogen is often integrated with ammonia synthesis due to hydrogen being difficult and energy-intensive to store and transport. Storage requirements typically include either high-pressure compression (172-690 bar) at room temperatures or cryogenic temperatures of -250 ºC at 1 atm. Hydrogen's low ignition energy and flame speed also introduces considerable safety concerns (Reiter and Kong, 2011).

Ammonia can be used as a fuel itself, or in a dual-fuel applications. Dual-fuel applications, in general have received more attention due to their current utilization capabilities, while ammonia as a single fuel is still under development. Common dual-

fuel applications are designed to operate with diesel, ethanol, hydrogen or methane. Ammonia is usually used as a secondary fuel, while–diesel works as the ignition fuel. Diesel-ammonia as a dual-fuel has become a widespread application especially in the marine industry, where large SCR systems, similar to mobile diesel applications, are already used to treat NO_x emissions (Reiter and Kong, 2011; Nova and Tronconi, 2014).

3 SELECTIVE CATALYTIC REDUCTION

3.1 Reaction network

The Selective Catalytic Reduction (SCR) is a method for the reduction of NO_x by ammonia in exhaust gases of stationary or mobile applications with high selectivity for N_2 formation. With the addition of reductant (ammonia) into the exhaust gas, NO_x will selectively react with NH_3 to form nitrogen and water and to a much less other gaseous compounds. NH_3-SCR consists of the following reactions (1-8):

$$4\ NO + 4\ NH_3 + O_2 \rightarrow 4\ N_2 + 6\ H_2O \quad (1)$$

$$NO + 2\ NH_3 + NO_2 \rightarrow 2\ N_2 + 3\ H_2O \quad (2)$$

$$4\ NH_3 + 3\ NO_2 \rightarrow 3.5\ N_2 + 6\ H_2O \quad (3)$$

$$4\ NH_3 + 3\ O_2 \rightarrow 2\ N_2 + 6\ H_2O \quad (4)$$

$$4\ NH_3 + 3\ O_2 \rightarrow 4\ NO + 6\ H_2O \quad (5)$$

$$2\ NH_3 + 2\ O_2 \rightarrow N_2O + 3\ H_2O \quad (6)$$

$$2\ NH_3 + 2\ NO_2 \rightarrow N_2O + N_2 + 3\ H_2O \quad (7)$$

$$2\ NO + O_2 \rightleftharpoons 2\ NO_2 \quad (8)$$

Equations (1)– (3) represent the main NH_3-SCR reactions. Equation (1) corresponds to the standard SCR reaction, Equation (2) describes the fast SCR reaction, and Equation (3) represents the NO_2-SCR reaction. Equations (4)– (8) describe the oxidation reactions with ammonia. Equation (4) represents the oxidation of ammonia to N_2, In Equation (5) the oxidation of ammonia to NO, and Equation (6) the oxidation of ammonia to N_2O are presented. Equation (7) describes the oxidation of ammonia by NO_2, while Equation (8) represents the formation of NO_2 from NO (Maunula et al., 2020; Ayodhya and Narayanappa, 2018).

The ratio of NO and NO_2 affects the dominant NH_3-SCR reaction. With a ratio of 1:1, fast SCR reaction dominates, whereas with NO only (Equation (1) and with a ratio higher than 1:1, Equation (3) starts to dominate. N_2O is a powerful greenhouse gas, of which emissions are included in reporting total GHG emissions (Ayodhya and Narayanappa, 2018).

3.2 NH_3-SCR catalysts

Common catalysts used in commercial NH_3-SCR systems are copper and iron deposited in the zeolite framework as well as vanadium pentoxide (vanadia, V_2O_5) supported on TiO_2. Major factors affecting the performance (activity, selectivity and stability) of the catalysts are associated with their chemical composition, morphology, preparation methods along with the reaction conditions (temperature, pressure, feed composition and space velocity). Major inhibiting/deactivation issues regarding NH_3-SCR catalysts are usually hydrothermal, chemical (e.g. sulphur), and hydrocarbon caused deactivation (coking) (Nova and Tronconi, 2014; Liu et al., 2020).

3.2.1 *Zeolite-based iron and copper catalysts*

Iron- and copper-based zeolites are well known and widely researched as NH_3-SCR catalysts. Generally, iron zeolites characteristics vary according to their respective zeolite structure and composition, but they share still a common trait, such as the high NO_x conversions at higher temperatures (ca. 400-550 ºC) and the good resistance against sulphur poisoning and hydrothermal aging. Fe-zeolites show a high promotion for NO_2 formation (Metkar et al., 2012) Copper zeolites show excellent performance in low-temperature NH_3-SCR and excellent hydrothermal durability at high temperatures, ca. up to 800 °C, but their use has performance limitations regarding sulphur exposure or poisoning. Copper-based zeolites generally provide better conversion in low temperature ranges (ca. 200-350 ºC). Generally, Cu-zeolites have a very high NH_3 adsorption capacity as well as low NO_2 promotion efficiency, which make them ideal for many low-temperature mobile diesel applications (Metkar et al., 2012; Maunula and Wolff, 2016).

The zeolite structure can affect many important factors regarding NH_3-SCR reactions, such as durability, ammonia adsorption capacity and NO_x reduction activity. Cu-zeolites are the mostly used worldwide in vehicle and machinery applications due to their good low-temperature performance, low NO_2 formation, and good hydrothermal stability (Nova and Tronconi, 2014; Maunula and Wolff, 2016).

Common support structures for iron- and copper-based catalysts include the ZSM-5 (MFI), Chabazite SSZ-13 (CHA), and Beta (BEA) zeolites (Martín et al., 2017; Sun et al., 2021; Abdul Nasir et al., 2024). ZSM-5 and BEA zeolites have a solid foundation as commercial catalyst supports, being well researched and developed during the past decades. They generally exhibit a high SCR efficiency but have a poor hydrothermal stability. On the other hand, CHA zeolites offer similarly a high SCR efficiency, but they generally possess a much higher hydrothermal stability. (Martín et al., 2017) Important characteristics of the zeolite supports include: Si/Al ratio, acidity and pore size distribution, which affect SCR efficiency, hydrothermal stability and poison resistance (Martín et al., 2017) Sun et al., 2021).

Currently, it has been recently under a lot of debate the iron site's structure and oxidation states being the most active in the ammonia adsorption and SCR reactions, and the important elementary steps in the reaction mechanism. Fe-zeolites appear to depend on the NO_2 formation promotion effect for the low and medium temperature SCR performance. (Maunula and Wolff, 2016; Abdul Nasir et al., 2024).

3.2.2 Vanadium-based catalysts

Vanadium-based or V_2O_5-WO_3/TiO_2 catalysts are well known and practiced NH_3-SCR catalysts developed for stationary and mobile NH_3-SCR applications. They have been used commercially for NO_x reduction in power plants first in Japan in the 1970s. (Lai and Wachs, 2018; Nova and Tronconi, 2014). In mobile applications, V-SCR was the main application in Euro 4 and Euro 5 levels before zeolite-SCR catalysts emerged as the mainstream SCR concept in Euro 6 level (Nova and Tronconi, 2014).

The vanadia catalysts are generally supported by the TiO_2 structure and often accompanied by either WO_3 or MoO_3 additives to improve their performance regarding thermal stability and NO_x conversion (chemical and structural promoters) (Lai and Wachs, 2018; Nova and Tronconi, 2014). Generally, supported vanadium catalysts composition is 1-3 wt%V_2O_5, 10 wt% WO_3 and the rest is the porous TiO_2 support. The V-SCR catalyst generally operates around the temperature window of 250-500 ºC. Other variations regarding the catalyst compositions exist as well, where common co-catalysts

added are cerium (Ce), manganese (Mn), iron (Fe) or copper (Cu). Ce and Mn are usually added to increase NO_x conversion at low temperatures. Fe and Cu might also create promotion in relation to their SCR properties (Nova and Tronconi, 2014; Ye et al., 2022).

Vanadium catalysts are particularly prone to oxidating sulphur compounds leading to N_2O at higher temperatures. Modern vanadium catalysts exhibit improved resistance against thermal aging, which had been an issue in the past. At higher temperatures (>600 ºC), TiO_2 support structure starts to sinter, which limits its use at higher temperature deNO_x applications, for example in modern after treatment systems (ATS) with DOC+DPF+SCR (Nova and Tronconi, 2014). Sulphur compounds, especially SO_2 and SO_3 are a major impediment in many vanadium SCR catalytic applications (marine, power plants-, high-S fuels), especially at lower temperatures (180 °C) due to the formation of ammonium sulphate ($(NH_4)_2SO_4$) and ammonium bisulphate (NH_4HSO_4), which cover active sites of the catalyst, thus reducing SCR performance (Lai and Wachs, 2018; Ye et al., 2022).

Vanadium-SCR catalysts generally exhibit a low resistance against thermal and hydrothermal aging due to sintering, which has been attributed to the decreased specific surface area of the TiO_2 support structure. Sintering decreases the specific surface area of the catalyst which in turn lowers conversion of NO_x (Nova and Tronconi, 2014; Beale 2015).). In addition to surface collapse by the rutile formation from high-surface-area anatase TiO_2, vanadium oxide oxidation state follows an irreversible change ($V^{5+} \rightarrow V^{4+}$, V^{3+}), which transformation was managed to shift to higher temperatures by the development of TiO_2 based vanadium catalysts (Maunula et al., 2013, Beale et al., 2015).

Alkali (e.g., Na, K) and alkaline (e.g., Mg, Ca) metals are also known to affect NO_x conversion adversely. These effects usually come from vanadium, forming harmful compounds, which block and inhibit active sites needed for ammonia adsorption and NO_x conversion (Chen et al., 2011). Alkali metals are known also to decrease the acidity of the catalyst, which further leads to catalyst deactivation by suppressing the ammonia adsorption. Common deactivating metals include also caesium (Cs) and magnesium (Mg) (Lisi and Cimino, 2020).

Similarly to alkali and alkaline metals, vanadium-based catalysts performance is also adversely affected by heavy metals. Heavy metals are usually associated with power plants or boilers emissions, due to the use of coal as fuel, since heavy metal traces are more common in these applications. The effect of heavy metals on the catalysts differs, some can be treated to restore catalyst performance, such as mercury (Hg) or selenium (Se), but heavy metals such as lead (Pb) or arsenic (As) are known to cause irreversible damage to the vanadium-based catalysts. Lead (Pb) is known to decrease NO_x conversion significantly. Lead is known to accumulate on the catalyst surface over time and to decrease NH_3 adsorption capacity. It occurs due to the formation of compounds such as lead(II) oxide (PbO) or lead(II) chloride ($PbCl_2$) which affect the SCR reaction negatively by either reacting with active sites or reducing surface acidity and reducibility of V^{5+} sites. Arsenic is forming harmful arsenic species such as As_2O_5 on the catalyst surface that can block or destroy active sites by either forming compounds on active sites or by physically forming a film layer on the catalyst surface (Wu et al., 2023; Szymaszek et al., 2020).

3.2.3 NH_3-SCR catalysts structure

NH_3-SCR catalysts can be manufactured in a variety of forms, each suited for specific circumstances according to the needed characteristics and conditions of the application. Commercially, the most widespread geometrical form in catalyst's structure is the honeycomb, while other common geometrical forms to include plate and corrugated catalysts. The catalyst structure is also strongly related to the catalyst carrier (ceramic, metallic, extruded) (Heck et al., 2009; Ye et al., 2022).

Honeycomb shape is a preferred geometrical form employed in SCR applications due to the symmetric structure, preparation method (extrusion) and varying dimensions needed for the application. These flow through structures offer higher efficiency regarding flow rates and resistance against mechanical and thermal attrition. (Bardhan, 1997; Heck et al., 2009; Ye et al., 2022). Commercial monolith catalysts are usually composed of either ceramic or metallic materials, of which the ceramic form is commercially more widespread (Heck et al., 2009; Ye et al., 2022).

Plate catalysts usually consist of metallic plates which are supported parallel to each other. The corrugated catalyst is a combination of straight and corrugated plates, which are made

from metallic folios or fibre mats rolled to a substrate structure. Metallic catalyst supports offer higher mechanical durability, thermal conductivity and thinner walls, which result in faster reaction light-off temperatures and lower weight compared to ceramic ones. However, they are more expensive than ceramic catalysts. Ceramic substrate catalysts are inexpensive and offer a high specific surface area but suffer from lower durability (Heck et al., 2009; Ye et al., 2022).

The cell density has a huge impact on the SCR reaction. Higher cell density translates to higher geometric surface area which means more surface for catalyst coating and lower external diffusion limits. Low density substrates are used in applications with high amounts of solid particles or in high dust applications and high cell density substrates are used in low dust applications in stationary or mobile SCR systems. (Ye et al., 2022)

3.3 NH_3-SCR applications

NH_3-SCR catalytic systems were originally designed for the aftertreatment of stationary exhaust gas streams such as those in powerplants and large marine applications, while mobile sources were related mainly to the automotive industry. Stationary and mobile NO_x control applications are similar in principle, although the concentration of each pollutive and harmful gas in the flue gas stream varies. Regarding structural differences, stationary and mobile NH_3-SCR systems share a similar layout with each other, differing slightly in application as well as in size (Nova and Tronconi, 2014; Ye et al., 2022).

The main differentiating factor between stationary and mobile applications is the fuel type, size, and operating temperature encountered. Large engine applications generally use low-quality fuels because of their lower cost. Major affecting factors regarding fuel include the amounts of ash and sulphur which affect, and limit, catalyst performance adversely as mentioned in Chapter 3.2. Aftertreatment devices for mobile sources suffer from space constraints in automotive industry and small marine applications. Exhaust temperature differences due to low speed (stationary) and high speed (mobile) applications also change the aftertreatment system (ATS) configurations since at lower temperatures the SCR catalyst is closer upstream to reach higher efficiency (Nova and Tronconi, 2014; Ye et al., 2022).

3.3.1 Stationary and marine applications

Stationary applications using NH_3-SCR include large combustion engines, such as in marine, power generation, and various boiler equipment used for thermal energy production, which eventually produce NO_x emissions. Because of the variety of applications and the differences in exhaust gas compositions, many variations in the catalysts design exist. These variations affect the choice of the active catalyst based on the needed properties such as temperature and poisoning resistance which influence NO_x conversion and catalyst lifetime (Nova and Tronconi, 2014; Heck et al., 2009; Ye et al., 2022).

Originally designed for diesel power plant applications, variations of these designs have been later adapted for the modern marine and other large engine applications, leading in different design approaches according to application requirements and environmental restrictions such as Euro 5 and Euro 6 goals. For marine applications, TIER III limits are applied which limit the NO_x emissions by engine size categories according to the engine's rpm (rotations per minute) ranges (Nova and Tronconi, 2014; Zannis et al., 2022).

The fuel source of the power plant also affects the catalyst's performance used since different impurities affect its performance and lifetime. Coal and heavy oil as fuels usually contain sulphur which can affect certain catalysts compositions. Biomass, on the other hand, can contain alkali metals such as potassium or magnesium which is also harmful to certain catalysts compositions (Ye et al., 2022).

As a typical example, the coal boiler exhaust system consists of the NH_3-SCR section, electrostatic precipitator (ESP) or hot side electrostatic precipitator (H-ESP), flue gas desulfurizer (FGD), air heater (AH), and heat exchangers. Electrostatic precipitator is used to remove ash from the flue gas, while flue gas desulphurizer is used to remove sulphur dioxide (SO_2) from the flue gas. Air heater is used to cool the flue gas and to save heat (optimize energy savings). The heat exchanger is used to convert liquid water into steam for an increased energy efficiency of the whole process. The stack is used to exhaust the flue gas (Miller, 2017; Heck et al., 2009).

In coal power plants NH_3-SCR systems can also be divided into high and low dust systems as well as tail-end systems. These configurations have different locations regarding the

SCR placement. In the case of coal fired boiler applications, SCR placement is shown in Figure 1 (Miller, 2017; Heck et al., 2009).

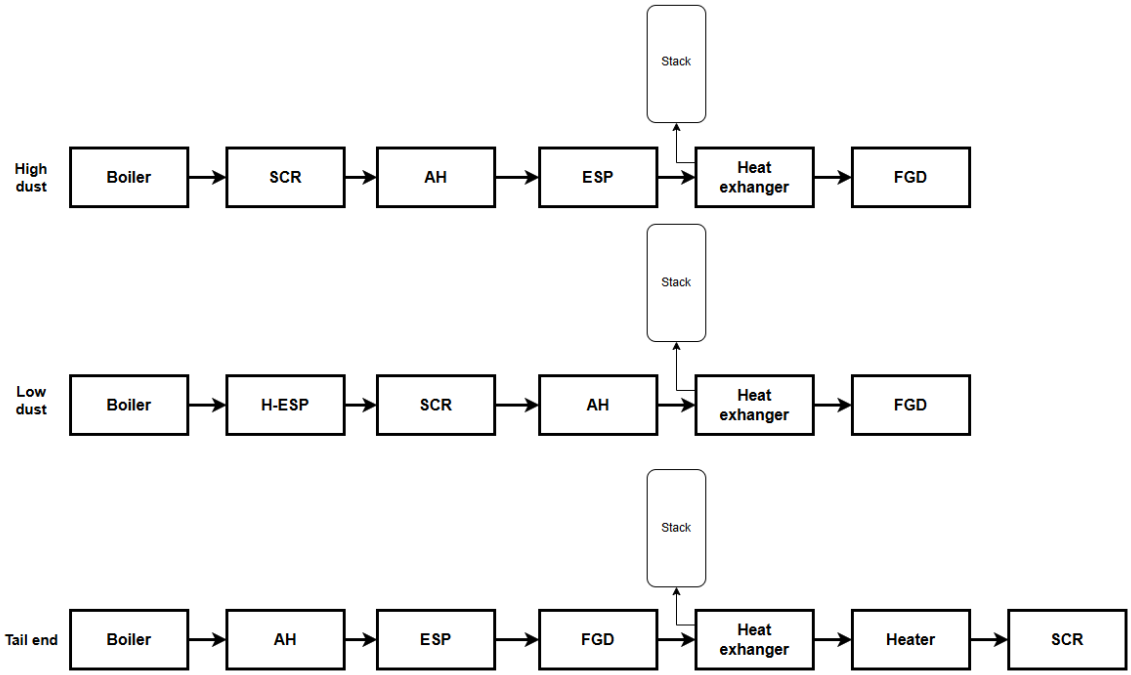


Figure 1. SCR boiler unit configurations for stationary coal-fired power plant (republished with permission of Miller 2017 © Elsevier).

High dust application usually refers to power plants, where the SCR system is placed just after the boiler for maximum heat recovery. High temperatures in the boiler hinder the utilization of heaters in flue gas downstream. As a drawback, if biomass is used as fuel, the catalysts usually wear down faster because catalyst surfaces were covered by particulates (PM, soot, alkali metals) (Ye et al., 2022; Miller, 2017; Heck et al., 2009).

In low dust applications, the SCR system is placed after the H-ESP which saves it from adverse effects of particulate matter. Unlike with high dust systems, low dust systems require additional heating costs due to H-ESP is more expensive to use than the regular ESP (Ye et al., 2022 Miller, 2017; Heck et al., 2009).

In the case of tail-end applications, the SCR system is placed downstream, after the electrostatic precipitator and desulphurization units. This application saves the SCR catalyst from dust and SO_2 effects but limits NO_x efficiency due to lower operating temperatures. Like low dust applications, tail-end systems require additional heating (Miller, 2017; Heck et al., 2009).

Marine or ship applications are their own non-wheels field, in where the V-SCR catalyst is usually the main aftertreatment systems (ATS) (Fig. 2). Marine SCR aftertreatment systems can be divided into low-pressure (LP-SCR) and high-pressure (HP-SCR) systems (Fig. 3). Structurally, the SCR system and the mixer placement is different in both applications. In LP-SCR, the system is placed after the turbine while in the HP-SCR case the catalyst is placed before the turbine. HP-SCR system in general is viewed as a more viable option regarding general increase in efficiency and emission conversion when the SCR system can utilize heat coming from the engine which is favourable for SCR reaction. To reach the Tier III NOx limits, it is important to maintain the optimal SCR temperature. LP-SCR system is limited in its use regarding fuel usage, having major effects by sulphur included in the fuel, whereas HP-SCR systems are more tolerant regarding sulphur containing fuel (Zannis et al., 2022). However, LP-SCR is the mainstream commercial SCR system, when it exists mechanical challenges in pre-turbo (HP) concepts.

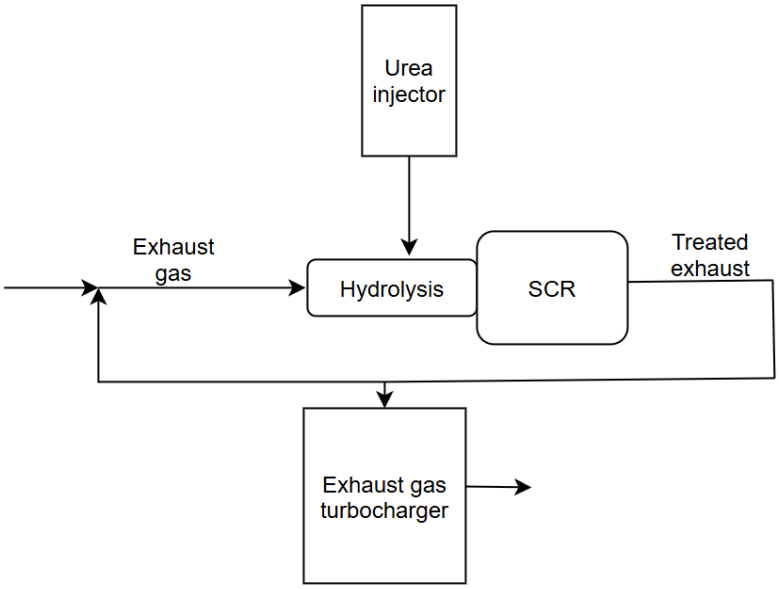


Figure 2. A marine aftertreatment system with pre-turbo SCR (Lu et al., 2020).

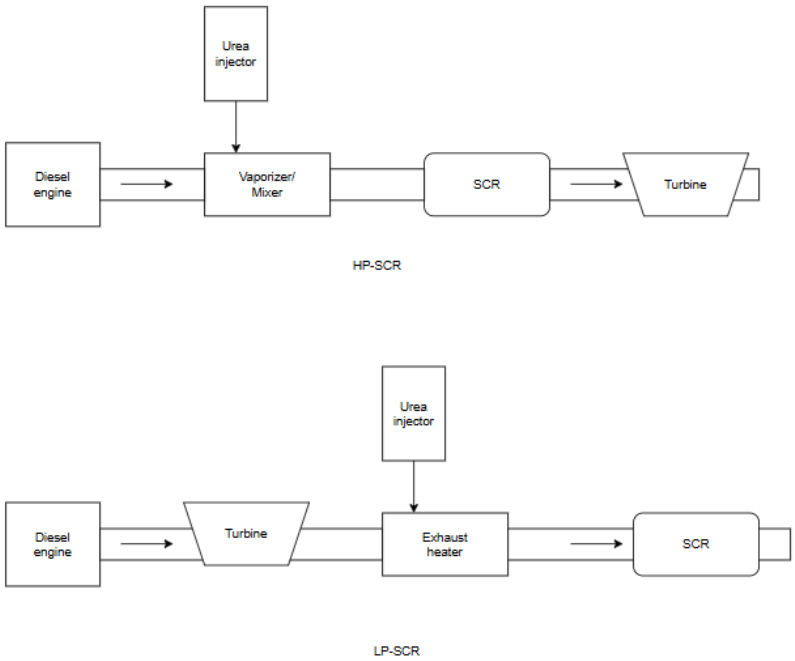


Figure 3. High- and low-pressure SCR systems typically used in marine applications (republished with permission of Zhu et al 2019 © Springer Nature).

3.3.2 Mobile SCR application – vehicles and nonroad machinery

Mobile applications for NH_3-SCR usually revolve around the automotive industry as well as medium-size machinery applications. (Nova and Tronconi, 2014).

Aftertreatment systems (ATSs) for diesel and dual fuel applications (Fig. 4) consist of diesel oxidation catalyst (DOC), diesel particulate filter (DPF), SCR-catalyst and the ammonia slip catalyst (ASC). DOC and DPF systems are more relevant to mobile applications due to tight emission limits for CO, HCs and PM (particulate matter). DOC is used for the oxidation of hydrocarbons (HC), carbon monoxide (CO) and NO, where NO_2 formation promotes the fast SCR reaction (Shan et al., 2021; Ayodhya and Narayanappa, 2018). An ASC is needed especially for ammonia fuelled engines or NH_3-SCR applications. Particulate matter compromises mainly of soot (C) ash, and sulphates (Nova and Tronconi, 2014; Ye et al., 2022).

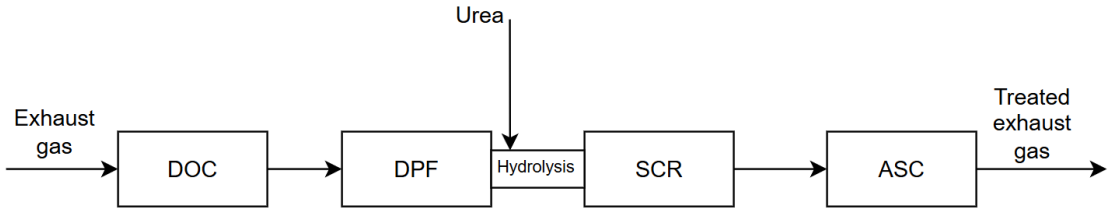


Figure 4. Typical mobile diesel ATS in Euro 6 applications (Shan et al., 2021 and Maunula et al., 2020).

TiO_2-based V-SCR catalysts were used mainly for mobile on-road applications in Euro 4 and 5. However, the tighter NO_x emission limits and development in zeolite-SCR compositions and durability results in the use of Cu- and Fe-SCR catalysts as a mainstream in Euro 6 light- and heavy-duty applications (Maunula and Wolff, 2016). Cu-zeolites suited particularly to light-duty applications including a long low-temperature city-driving periods in emission test cycles. The required NO_x conversions for SCR are usually over 90-95% to reach the latest emission limits (Euro 6, off-road Stage 5) in transient car, truck and machinery emission test cycles. Oppositely, the NO_x emission targets in marine applications on V-SCR catalysts are usually around 60-80% in steady engine points at the temperatures above 250 °C. SCR-catalyst related functions were discussed in Chapters 3.1 and 3.2 (Ayodhya and Narayanappa, 2018). Hydrocarbons adversely affect NO_x conversion which lowers the catalyst's conversion efficiency by inhibiting active sites (Ayodhya and Narayanappa, 2018).

4 AMMONIA ADSORPTION AND OXIDATION

4.1 Ammonia adsorption

The adsorption phenomenon of a chemical adsorbing compound (adsorbate) can be categorized according to the nature of a chemical solid phase (adsorbent) in contact. Interactions can occur between adsorbate in liquid phase and the adsorbent in the solid phase (liquid-solid) and between adsorbate in the gas phase and the adsorbent in the solid phase (gas-solid). (Dąbrowski, 2001). Adsorption phenomena can be also divided into physical adsorption (physisorption) and chemical adsorption (chemisorption). In the case of physical adsorption, the molecular species interact with the solid surface by van der Waals type of forces forming a multilayer of adsorbed species (more than one monolayer). The energy of interaction is very low, and this adsorption process is exothermic and reversible. In the case of chemical adsorption or chemisorption, there is a specific chemical interaction (formation of a chemical bonding) between atom(s) on the solid surface (adsorbent) and the gaseous molecular species (adsorbate). It is possible to encounter both types of physical and chemical adsorption simultaneously during an adsorption process at room and lower temperatures (Králik, 2014). At higher temperatures, only chemisorption is encountered in a gas-solid system, and the energy of interaction is significantly larger than that of physical adsorption.

The adsorption process of ammonia can be monitored using the transient adsorption method during which the sudden change of the concentration of the gas at the inlet of the adsorbent material (step-gas concentration switch) causes variations in the adsorbate concentration at the reactor outlet flow. Concentrations are monitored by online mass spectrometer (gas analyser). Based on this dynamic technique, the dynamic kinetic rates of adsorption and the amount adsorbed at equilibrium can be monitored. Details regarding the transient absorption method will be covered in Chapter 5.3.2.

4.1.1 Lewis and Bronsted acid adsorption sites

The current established theoretical background on ammonia adsorption is that NH_3 is bound on the catalyst surface on the Lewis and Bronsted surface sites, where weakly bound ammonia is occurred on Lewis acid sites and strongly bound ammonia is occurred

on Bronsted acid sites. Similarly, it is assumed that Lewis sites participate in the NH_3-SCR reaction, while the majority of ammonia adsorption capacity is linked to the Bronsted acid sites. It is claimed that on Bronsted acid sites ammonia is bound as NH_4^+ ions and for the Lewis acid sites as plain NH_3^* (Yao et al., 2012).

Ammonia adsorption depends on the physico-chemical properties of the surface of the catalyst, which are different for each catalyst. The nature of the active sites for ammonia adsorption, especially on V_2O_5 catalysts, are still under debate. It is known that TiO_2 surface can also provide Lewis acid sites, thus contributing to the ammonia adsorption phenomenon (Lai and Wachs, 2018). Ammonia adsorption during SCR reaction is observed in Figure 5 on the vanadium catalyst.

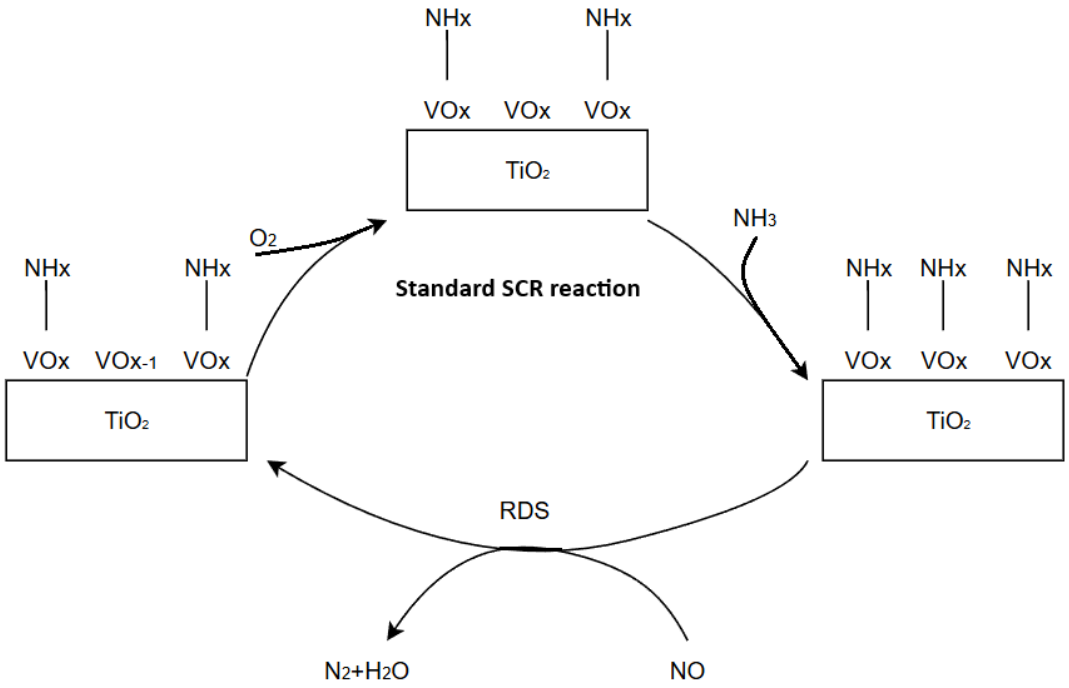


Figure 5 A schematic diagram of the standard SCR reaction on vanadium catalyst (republished with permission of Zhu, Lai, Tumuluri et al 2017© American Chemical Society.)

It is widely accepted that iron-based zeolites exhibit a wide variety of Fe species which participate in the adsorption process. It is also generally accepted that at lower temperatures the adsorption occurs on Fe^{3+}, while at higher temperatures on the oligomeric Fe_xO_y species. Fe^{3+} can also act as a Lewis acid site for ammonia adsorption, while silica offers mainly Bronsted sites. Similarly, the support structure of the catalyst, especially the Si/Al ratio, plays significant role on the adsorption phenomena due to the

amount of increased Bronsted sites as well as on the distribution of the iron species on the catalyst (Zhang, 2016).

4.1.2 Transient adsorption studies on vanadium-based catalysts

As the first commercially applied SCR catalyst, vanadium-based catalysts remain as a cornerstone of modern NH_3-SCR research. Most studies focused on the conventional V_2O_5-WO_3/TiO_2 compositions and their modifications. Although this traditional catalyst has been extensively investigated, ongoing research continues to explore new additives and improvements.

Kleeman et al. (2010) investigated three different commercial Vanadium SCR catalysts, of which two were coated and one was extruded. Ammonia adsorption experiment was conducted first in a flow of 1000 ppm NH_3 at varying temperatures between 200 °C to 450 °C in steps of 50 °C until the catalyst was fully saturated. Through ammonia desorption measurements from the catalyst surface, ammonia adsorption capacities were determined. Between the extruded and coated V_2O_5-WO_3/TiO_2 catalysts there were major differences in the adsorption capacities. Extruded catalyst outperformed the coated catalyst on adsorption capacity under the adsorption conditions applied at almost every temperature, except for 400 and 450 °C, where coated catalyst performed better. On the ammonia adsorption capacity, the comparison was reasonable since the catalyst amount is usually about 3-4 times higher in extruded (400-500 g/L) than in coated catalysts (150-200 g/L).

4.1.3 Transient adsorption studies on iron-based catalysts

Iron–zeolite SCR catalysts have been extensively studied over many years. They are often compared with other SCR-catalysts such as copper-based zeolites, as well as with their predecessors, vanadium-based catalysts. As noted in Chapter 3.2.1, zeolite support structures vary, which means that experimental conditions and results obtained are rarely identical when compared between different studies.

Grossale et al. (2008) tested the ammonia adsorption capacities of commercial vanadium and iron zeolite catalysts. The iron zeolite was a coated honeycomb monolith with a cell density of 400 cells per square inch, and with the catalyst amount of 0.262 wt% on monolith. The catalyst was tested both as ground material and with a small monolith piece. The V-SCR catalyst was used as a comparison similarly in ground and in monolithic form. Experiments were conducted in the temperature ranges of 50-200 °C while the gas flow contained helium, oxygen, water and 1000 ppm NH_3. Adsorption capacities were measured based on the amount of active phase present (gram per active phase of the catalyst or mol/g_{cat}). It was found that Fe-zeolite catalyst adsorbed more ammonia than V-SCR catalyst at all temperatures (Grossale et al., 2008).

Høj et al. (2009) tested different Fe-SCR catalyst types to determine the effect of atomic iron on SCR. Adsorption capacities for different Fe-BEA catalysts with low to high iron loadings (0.28%, 0.90%, 1.20%, 2.60%) were tested by performing TPD. The sample (200 mg) which was initially in a hydrated state, was first dried at 150 °C for 30 min followed by adsorption with 2% NH_3 in He at 150 °C, and using a flowrate of 150 Nml/min. After adsorption the sample was flushed with nitrogen at the same temperature, followed by cooling in N_2 to 110 °C after which TPD was started. TPD was run at the rate of 5 °C /min until it reached 750 °C, where it was then kept isothermally for 30 min. After cooling the dry weight of the catalyst was measured. Adsorption capacities showed minor differences between each other, but TPD profiles were used to confirm that at the Fe loadings between 0.28-1.2%, adsorption was dominated by iron in atomic state (Høj et al., 2009).

Shwan et al. (2014) compared the effects of hydrothermal aging on Fe-BEA and H-BEA catalysts. The two catalysts were investigated to determine the effect of hydrothermal aging on the catalyst structure and to create a kinetic model that could predict catalyst deactivation mechanism influenced by the hydrothermal aging performed on the catalysts. Both Fe-BEA and H-BEA catalysts were prepared in monolithic form with Fe-BEA having 1 wt.% Fe content and with cell density of 400 cpsi and a diameter of 21 mm and length of 20 mm. Fe-BEA samples were treated at 700 °C for 3 and 24 h, and H-BEA sample was treated only at 600 °C for 24 h. Fresh samples without hydrothermal aging were also prepared for comparison. Before adsorption, all samples were treated in

8-vol% O_2 in argon gas for 8 min. At the adsorption stage of the experiment, the samples were introduced to 400 ppm NH_3 and 5% H_2O at 150 °C for 40 min, after which they were isothermally desorbed at 150 °C with 5 vol% H_2O in the feed for 30 min. After isothermal desorption, the temperature of the samples was increased linearly at the rate of 10 °C/min until it reached 500 °C, where a base line was reached (no further desorption). The GHSV used for the experiment was 27,600 h^{-1}. Fresh H-BEA had higher ammonia adsorption than hydrothermally aged Fe-BEA. In the case of Fe-BEA catalysts, hydrothermal aging had little effect on the rates of isothermal desorption, but hydrothermal aging had a major deactivating effect on both catalysts. An effect observed between 3 and 24h of hydrothermal aging on the Fe-BEA during TPD was less prominent than on the fresh sample (Shwan et al., 2012).

4.1.4 Moisture effect on NH_3 adsorption

There is currently a lot of debate regarding the role of water in the adsorption of ammonia during NH_3-SCR processes. Some studies support the claim that the presence of water inhibits ammonia adsorption due to competitive adsorption between water and ammonia molecules on active sites. Similarly, water is thought to alter the distribution of Lewis and Bronsted acid sites on the catalyst surface, which sites are essential for the ammonia adsorption capacity. Water may also contribute to catalyst deactivation over time through swelling, vaporization, or the formation of harmful compounds, especially in the presence of alkali metals. Also, some studies suggest otherwise, that water can enhance ammonia adsorption under certain conditions. This effect is often attributed to the increase in the concentration of Bronsted sites on the catalyst surface, which would affect the adsorption phenomena positively (Szymaszek et al., 2020; Lai and Wachs, 2018).

Shi et al. (2018) investigated the effects of water vapour on commercial Fe-BEA catalysts. They reported that the addition of water vapour increased the amount of Bronsted acid sites, which inhibited regular NH_3-SCR reaction. They performed multiple experiments with and without the addition of water in the emission gas composition. Experiments were conducted in a fixed-bed quartz tube reactor at the temperature range of 100-650ºC. Gas composition included NO, NH_3, O_2, N_2 and H_2O vapor, while GHSV was kept at 60,000 h^{-1} (Shi et al., 2018).

Liu et al. (2019) have investigated the effects of water on the reaction pathways and active sites on the commercial vanadium SCR catalyst. Experiments were conducted using the transient response method. They reported that the addition of H_2O in the feed increased the adsorption capacity of ammonia on the catalyst at 150 °C. This was thought to be due to an increase in the Bronsted acid sites of the catalyst surface.

Lott et al. (2024) have studied the effect of water contents in simulated internal combustion engine conditions over a commercial vanadium catalyst. The water content in the feed was 10 and 20 vol% while the adsorption temperatures used were 180 and 300 °C. The catalysts were also aged to compare the difference between fresh and aged samples. They reported non-existent effect of water on the adsorption capacity of both fresh and aged VWTI samples. Aging also affected the adsorption capacity negatively, decreasing the adsorption capacity about 20-25% (Lott et al., 2024).

Grossale et al., (2008) similarly investigated the differences between Fe and V-SCR catalysts in different NH_3-SCR conditions, such as SCR in the presence of water. Experiments were conducted using 1000 ppm NH_3, 2 vol% O_2 and 1-10 vol% H_2O feed conditions, while the temperature during adsorption was kept at 200 °C. They reported that water had no effect on ammonia adsorption capacity on both Fe- and V-SCR catalysts.

4.2 Ammonia oxidation reaction

Ammonia oxidation is a well-known reaction especially in the field of nitric acid production and as a part of NH_3-SCR reactions in aftertreatment systems, the difference being in the concentrations in each process (vol% vs ppm range). Ammonia oxidation mainly compromises the oxidation step from NH_3 to NO, but different side reactions are known to occur, such as formation of N_2 and N_2O as described in the Equations (4)– (8). The main competing steps are known to be those between the NO and N_2 formation, while the formation of N_2O is usually linked with conditions at higher partial pressures (Scheuer et al., 2009).

Platinum as an active metal is a well-researched oxidation catalyst especially regarding nitric acid production in higher volumes and as a part of emission after treatment systems

(ATS). Usually, it is employed as part of an ATS system and forming NO_2 for the SCR process. Pt-DOCs are usually based on alumina-based supports and employed at higher spatial velocities such as 100,000-500,000 h^{-1}, but the design can vary depending on the application. Regarding ASC compatibility, platinum usually deposited on alumina-based supports, is known as a very active metal for the oxidation catalyst layer due to its durability and requirements for small volume. The Pt loading for the ASC systems requirements is generally around 2-5 g/L, and the volume is about 5-15% of the SCR catalyst volume. Regarding the selectivity and activity of the Pt catalyst, it is usually favoured to be on the smaller particle size due to lower activity but higher selectivity regarding N_2 formation (Scheibe et al., 2005; Imbihl et al., 2007).

5 EXPERIMENTAL

5.1 Catalysts

The investigated catalysts are related to SCR (V, Fe) and ammonia oxidation (Pt) for marine applications. Catalysts used for the transient and other experiments conducted consisted of four different catalysts compositions, namely: V-SCR-1, V-SCR-2, Fe-SCR and Pt-DOC, and a catalyst mixture (physical mixing) consisting of 90% V-SCR1 and 10% Pt-DOC. Respective physical characteristics of the catalysts are described in Table 1.

Table 1. Catalyst samples used in the experiments and their physical characteristics.

Sample	Type	Composition	Coating (g/dm^3)	Cell density (cpsi)	Catalyst (wt-%)	Pretreatment temperature (°C)
V-SCR-1	Extruded	V_2O_5- WO_3/TiO_2	-	60	100	450
V-SCR-2	Coated	V_2O_5- WO_3/TiO_2	124	400	29,2	450
Fe-SCR	Coated	Fe-Beta	141	400	32.0	750
Pt-DOC	Coated	Pt/Al_2O_3	118	400	28.2	450

The samples were prepared from larger honeycomb catalysts at the University of Oulu. The final samples consist of catalyst in powder form, which were sieved to the particle sizes of <250 µm (minimize internal mass transport effects). Sample sizes for the individual catalysts were determined by the GHSV used in the experiments. Sample amount was quite similar in all reaction experiments (ca. 74-80 mg). The adsorption capacities by adsorption or desorption results were calculated over the efficient catalyst amount (by catalyst wt%) in samples.

5.2 Texture characterization of catalysts

The texture characterization of the various catalysts was performed using the Brunauer-Emmett-Teller (BET) method to determine specific surface area (m^2/g), and the BJH (Barret-Joyner-Halenda) method for determining the mean pore size (d_p, nm) and specific volume (cm^3/g) of the porous catalytic systems. Characterizations were performed using

a Micromeritics ASAP2020 analyser at the laboratory of Environmental and Chemical Engineering at the University of Oulu.

5.3 Transient kinetic experiments setup

5.3.1 Gas flow and reactor system

A variety of transient kinetic experiments were conducted at the Heterogenous catalysis laboratory – Chemistry Department of the University of Cyprus using a home-made specially designed gas flow system coupled with a heated micro-reactor system connected to a quadrupole (Balzers, 1-300 amu, atomic mass unit) mass spectrometer having a fast response inlet capillary/leak diaphragm system. The transient gas flow system consisted of eight mass flow controllers which were connected to respective gas canisters and the pneumatic gas switching valve used for the precise step gas concentration change between gas mixtures of different compositions in the inlet of the microreactor connected to the mass spectrometer (Fig. 6 and 7). Temperature within the reactor was controlled by a PID temperature controller while a thermocouple (1/16 in od) was placed inside the reactor in contact with the catalytic bed and which measured the gas temperature in the catalytic bed (Fig. 8).

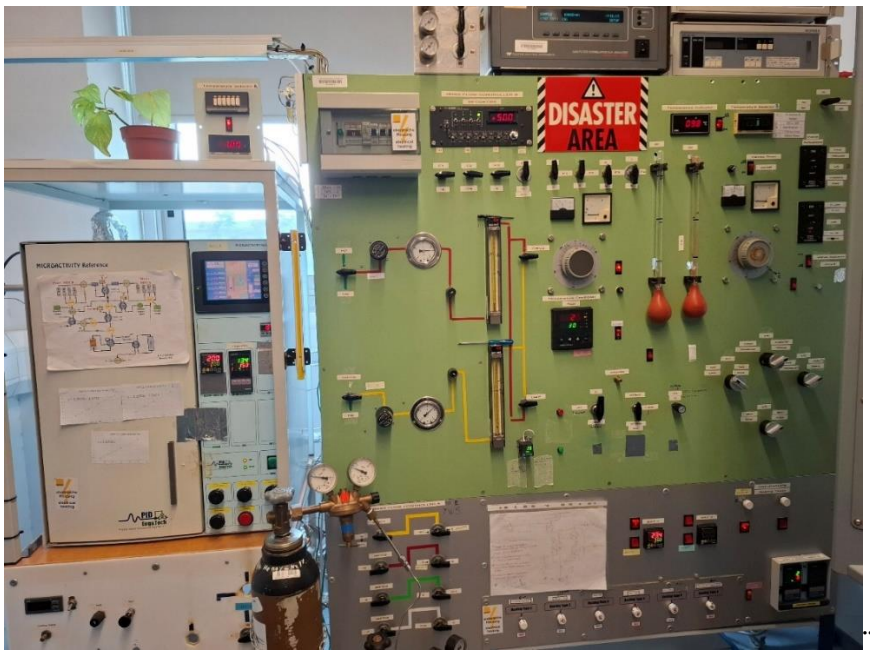


Figure 6. Gas flow system for applying the Transient Method at the heterogeneous catalysis lab - Chemistry Department of the University of Cyprus.



Figure 7. The gas cylinders storage compartment used for the supply of gases to the transient gas flow system.

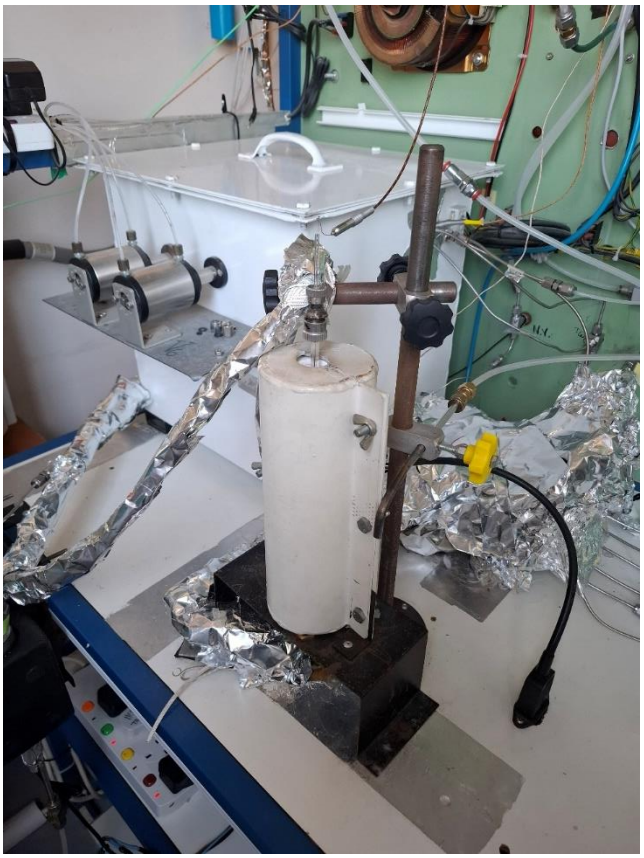


Figure 8. The heated microreactor connected to the transient gas flow system and the online mass spectrometer gas analysis system.

5.3.2 Mass spectrometry gas analysis

Mass spectrometry (MS) is an analytical technique for the qualitative and quantitative analysis of a gas mixture. A mass spectrometer usually consists of three parts: (a) Ion source, (b) mass analyser, and (c) charged ions detector. The ion source is responsible for producing positively charged ions of the gas constituents (by ejecting one or more electrons from its initial molecular structure by electron bombardment-ionization process). The mass analyser sorts out the ions by their mass to charge ratios (m/z). A detector is used for the measurement of the positively charged ions (nature and concentration), and their variations are plotted as a spectrum of intensity (current, μA) vs m/z every regular intervals of time (ca. 10 ms one of the shortest intervals) (Garg and Zubair, 2026; Urban, 2016). An on-line quadrupole mass spectrometer (Omnistar Balzers) was connected to the transient gas flow system close to the exit of the microreactor to record the fast gas concentration responses aiming to follow dynamic phenomena in a gas-solid catalytic interaction. Mass signals of NH_3 (15 m/z), N_2O (44 m/z), NO (30 m/z), N_2 (28 m/z) and H_2O (18 m/z) were recorded as a function of time in a variety of transient kinetic experiments designed and conducted as reported in the following Section 5.4.

5.4 Transient kinetic experiments

The transient kinetic experiments conducted were divided into four parts to capture the different experimental conditions and the purpose of performing them. All experiments were conducted using a GHSV of 31,200 h^{-1}. The experimental plan with all samples investigated and the conditions and feed gas concentrations used is presented in chapters below.

5.4.1 Ammonia adsorption/desorption on NH_3-SCR catalysts in dry conditions (TE1)

The first transient experiment (TE1) relates to the effects of adsorption temperature and ammonia feed concentration on the transient (dynamic) kinetic rates of adsorption and desorption, and on the ammonia adsorption capacity (equilibrium adsorption condition) as a function of catalyst composition. The obtained results between the three different catalysts investigated (V-SCR-1, V-SCR-2 and Fe-SCR) were analysed and compared

(Tables and graphs). The TE1 experiment consisted of three parts: (A) the isothermal adsorption stage (constant temperature), (B) the isothermal desorption stage at the same adsorption temperature in He inert gas, and (C) the temperature-programmed desorption in He gas (TPD) stage (Fig. 9).

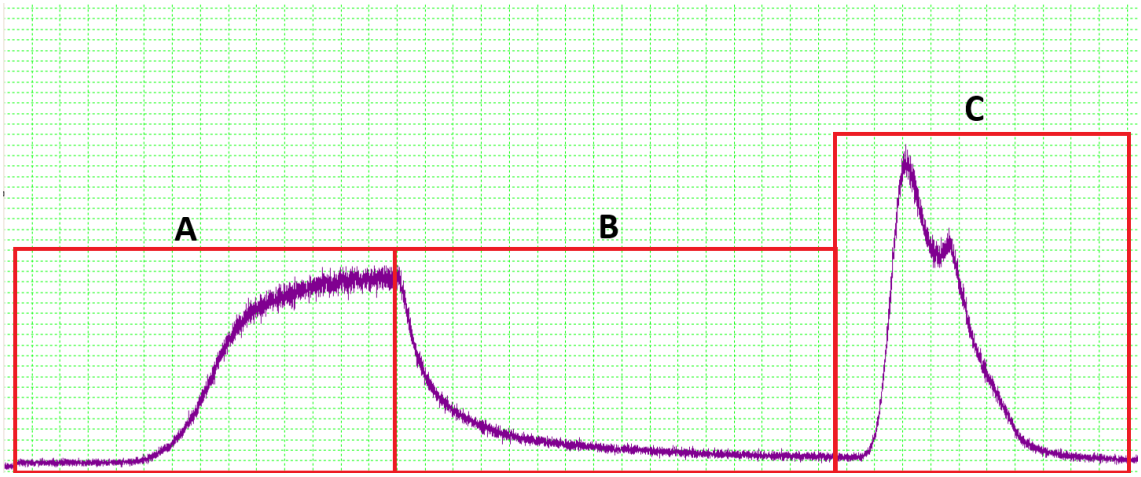


Figure 9. Isothermal ammonia adsorption (A), isothermal desorption (B) followed by TPD (C).

In the adsorption stage, the feed gas of certain (x) ppm NH_3 (x: 100, 300, 500 ppm) in He carrier gas was switched through the reactor system (He $\rightarrow$ x ppm NH_3/He (T, t)) at a total flow rate of 50 ml/min, while the temperature of the reactor was kept isothermal. Changes in the output concentration of ammonia and any other gases that might had formed were continuously monitored by online mass spectrometry. At the initial stage of the adsorption, no ammonia concentration was recorded at the outlet of reactor as depicted in (Fig. 9A), as the result of strong ammonia adsorption on the catalyst surface. As the time of adsorption increased, ammonia concentration in the outlet of reactor started to increase continuously in an exponential like manner, reaching a steady-state value after some time (Fig. 9A). At this point, the available catalytic sites adsorbing ammonia were saturated. Once saturation was reached, the flow of x ppm NH_3/He was switched to He (inert gas) to investigate the isothermal desorption characteristics of the system.

In the isothermal desorption stage (Fig. 9B) weakly bound ammonia species is removed (desorbed) from the catalyst surface. Similarly to the adsorption stage, the dynamic rate of desorption is directly linked to the decrease in the signal of ammonia. When the latter signal reached a very low value (Fig. 9B), a TPD of ammonia run was started as depicted in Figure 9C.

In the TPD run in He gas flow (50 mL/min), the temperature of the solid catalyst was gradually increased at the rate of 30 °C/min up to a maximum temperature (450 °C for V and 750 °C for Fe catalysts), and kept constant at least for 10 min or until the ammonia signal fully stabilized to its background value, after which the TPD run was stopped. In addition to NH_3, possible reaction products (surface reaction of adsorbed ammonia with the catalyst) were also monitored during all the stages of TE1. It is clearly observed in Figure 9C that two desorption peaks of ammonia were recorded, indicating that at least two adsorption sites with different binding energies for ammonia were present on the catalyst surface. According to the TPD theory, the lower the peak maximum desorption T the lower the binding strength of adsorption (Katada et al., 1997).

5.4.2 Effect of N_2O on ammonia adsorption (TE2)

In the transient experiment 2 (TE2), the same experimental procedure as in Transient experiment 1 (TE1) was followed, but the feed gas in the adsorption step included also 50 ppm N_2O. Isothermal desorption step along with TPD were conducted similarly to TE1. Signals of ammonia, N_2O and possible side products (NO, N_2) were monitored during this experiment. Experiments were conducted on V-SCR-1 and Fe-SCR catalysts.

5.4.3 Ammonia adsorption-oxidation in dry conditions (TE3)

In the transient experiment 3 (TE3), the surface reaction between pre-adsorbed ammonia species and gaseous oxygen was investigated. Following isothermal adsorption of ammonia (x ppm NH_3/He (T, t)), the feed was then switched to 5 vol% O_2/He (T, t). No TPD stage was conducted in this experiment. Catalysts used for the experiments included V-SCR-1, V-SCR-2 and Fe-SCR, and a mixture of Pt-based and V-SCR-1 solids. A Pt-based catalyst (Pt-DOC) was included to test the effect of an oxidation of ammonia catalyst in the presence of an ammonia adsorption catalyst (V-SCR-1) and simulate the ASC catalytic conditions.

5.4.4 Ammonia adsorption on SCR catalysts in wet conditions (TE4)

The effect of water on the adsorption of ammonia was investigated (TE4). A gas mixture of 500 ppm ammonia, 5 vol% H_2O and He as balance gas was used. Desorption in He carrier gas followed by TPD was conducted similarly as in TE1. Experiments were

conducted on the V-SCR-1 and Fe-SCR catalysts, and the obtained results were compared to those obtained in the absence of water in the adsorption gas (TE1).

5.4.5 Mass spectrometry analysis

Mass spectrometry signals (m/z, μA) recorded were first converted to concentrations (ppm or vol%) by using certified gas mixtures as a calibration procedure (Gui et al. 2025). These responses were used in appropriate material balances constructed to calculate dynamic (transient) rates of adsorption (Eq. 10) and desorption (Eq. 11) and amounts (mol/g) of adsorption and desorption.

By integrating the rates, we acquire the total amount of adsorbed or desorbed chemical constituents.

$$Z_{i(t)} = \frac{I - I^{bck}}{I^{bp} - I^{bck}} \quad (9)$$

$$R_ads = \frac{F}{w} * y_x * (Z_{Kr_{(t)}} - Z_{x_{(t)}}) \quad (10)$$

$$R_des = \frac{F}{w} * y_x * (Z_{x_{(t)}} - Z_{Kr_{(t)}}) \quad (11)$$

$$F_x\ (t)\ = \frac{I_x - I_x^{bck}}{I_x^{sens} - I_x^{bck}} * \mathrm{F} \quad (12)$$

$$Z_i = \frac{I_{NH3}}{I_x^{sens}} \quad (13)$$

The Zi(t) dimensionless parameter in equation (9) represents the conversion of the raw signal of a given gas i to a normalized concentration, which takes values between 0 (at the gas switch, t=0), and unity (after gas saturation conditions). The latter means that the signal at the exit of the reactor is the same as that in the feed gas stream. I is the raw signal, I^{bck} is the background signal in the carrier of the given m/z, I^{bp} is the signal of the gas in the feed gas stream. For example, using a feed gas stream of 500 ppm NH_3 and 1 vol% Kr (tracer gas) balanced with He, I^{bp} corresponds to the signal measured at m/z=15 for 500 ppm NH_3 (bypass the reactor), and at m/z=84 for 1 vol% Kr (bypass the reactor).

Equation (10) allows to estimate the dynamic rate of adsorption of a given gas, such as NH_3, during the adsorption stage of the transient experiment, where F is the total molecular flow (mols/s) of the feed, w is the mass of the catalyst used in the experiment, y_x is the mole fraction of the adsorption gas (e.g., ammonia) in the feed. $Z_{Kr_{(t)}}$ is the dimensionless concentration of krypton tracer gas, and $Z_{x_{(t)}}$ is the signal of the adsorption gas of interest (e.g., ammonia) at a given time during the transient experiment.

Equation (11) allows to estimate the rate of desorption of a gas during the isothermal treatment in He carrier, following the adsorption stage.

Equation (12) allows to estimate the molar flow rate, F_x (mols/s) of the desorbed gas during temperature programmed desorption, where I is the observed signal of the gas x, , I^{bck} is the background signal of the observed gas x (under He carrier gas), I_x^{sens} is the value of the signal for a standard calibration gas used (μA/ppm), and F is the total molar flow rate of He carrier gas used (mols/s). By integration of F_x (t) with time, the total amount of desorbed gas (mol/g) can be estimated.

Equation (13) allows the conversion of the processed signal (μA) into concentration (ppm or vol%), where I_{NH3} is the background signal of the observed gas and I_x^{sens} is the value of the signal in the certified calibration signal.

6 EXPERIMENTAL RESULTS

6.1 Catalysts characterization

BET measurements for catalysts' texture characterization were performed for the fresh samples after ground to powders. The coated samples included the catalyst and cordierite materials. For the estimation of textural parameters related only to the catalytic material, the known coating amount on cordierite substrate was considered (Table 2).

Fe-SCR catalyst presented the highest BET surface area while the extruded V-SCR-1 had the lowest value. V-SCR-2 and V-SCR-1 catalysts show the highest mean pore size which correlates to the lower surface areas. Fe-SCR (zeolite) and Pt-DOC (alumina) had the highest pore volumes and the highest BET values among the catalysts investigated.

Table 2. Texture characterization of V-SCR-1, Fe-SCR and Pt-DOC SCR catalysts.

Sample	Surface area (BET) (m^2/g catalyst)	Mean pore size (nm)	Pore volume (cm^3/g catalyst)
V-SCR-1	65	17	0.3
V-SCR-2	82	19	0.4
Fe-SCR	391	5	0.5
Pt-DOC	216	10	0.5

6.2 Ammonia adsorption on SCR catalysts in dry conditions

6.2.1 Effect of temperature

The transient response curves recorded in all experiments were analysed in terms of rates than concentrations, where simple integration of the rate with time provides the amounts of a gas adsorbed or desorbed. Also, it is very important to compare these dynamic rates among the series of catalysts to gather better insights into the adsorption/desorption processes of given gas over the tested catalytic SCR materials. It is very important to point out that two materials may have the same adsorption capacity (at equilibrium

conditions) but totally different dynamic rates. In other words, one material reaches the equilibrium state very fast while the second one very slow. This is a very important information that only transient adsorption and desorption kinetics can provide.

Figure 10 shows the transient rates vs time of ammonia adsorption (500 ppm NH_3/He) in the 150-400 ºC range over the V-SCR-1and Fe-SCR catalysts. Regarding V-SCR2, only TPD results were compared in TE-1 series. As clearly seen in all case for the initial short period of the experiment all the ammonia fed in the catalytic reactor was adsorbed (no ammonia signal was detected at the outlet of the reactor), thus a maximum in the rate of adsorption is estimated. This value is practically equivalent to the feed rate value of ammonia in the reactor (0.22 μmol NH_3/g/s).

Notable differences in the dynamic rates of adsorption appear in terms of the time required for complete saturation of the adsorption sites present in each catalyst as a function of adsorption temperature (Fig. 10). The extruded V-SCR-1 clearly shows the shortest time, and as a consequence of that, it exhibits the lowest amount (μmol/g) of ammonia adsorption compared to the Fe-SCR catalytic systems at all temperatures investigated (150-400 ºC).

Fe-SCR shows the longest time during which full adsorption of inlet ammonia takes place (highest adsorption rate) at all adsorption temperatures (150-400 ºC). It is very interesting to remark that Fe-SCR and V-SCR-1 show similar dynamic adsorption rate patterns for all temperatures (Fig. 10). This result can be explained by stating that the kinetics of ammonia adsorption is similar over the two catalysts, but the number of sites is significantly larger on Fe-SCR than V-SCR-1. This is true after comparing the area under the rate profiles, which is proportional to the amount of ammonia adsorption (μmol/g). The amounts of ammonia adsorption in the 150-400 ºC range are presented in Figure 10, where in the case of "isothermal adsorption" Fe-SCR (Fe-beta zeolite) shows by far the largest amounts of ammonia adsorption at all four temperatures investigated. It is widely known that iron zeolites generally exhibit higher ammonia adsorption capacities than V-SCR (Maunula, 2013).

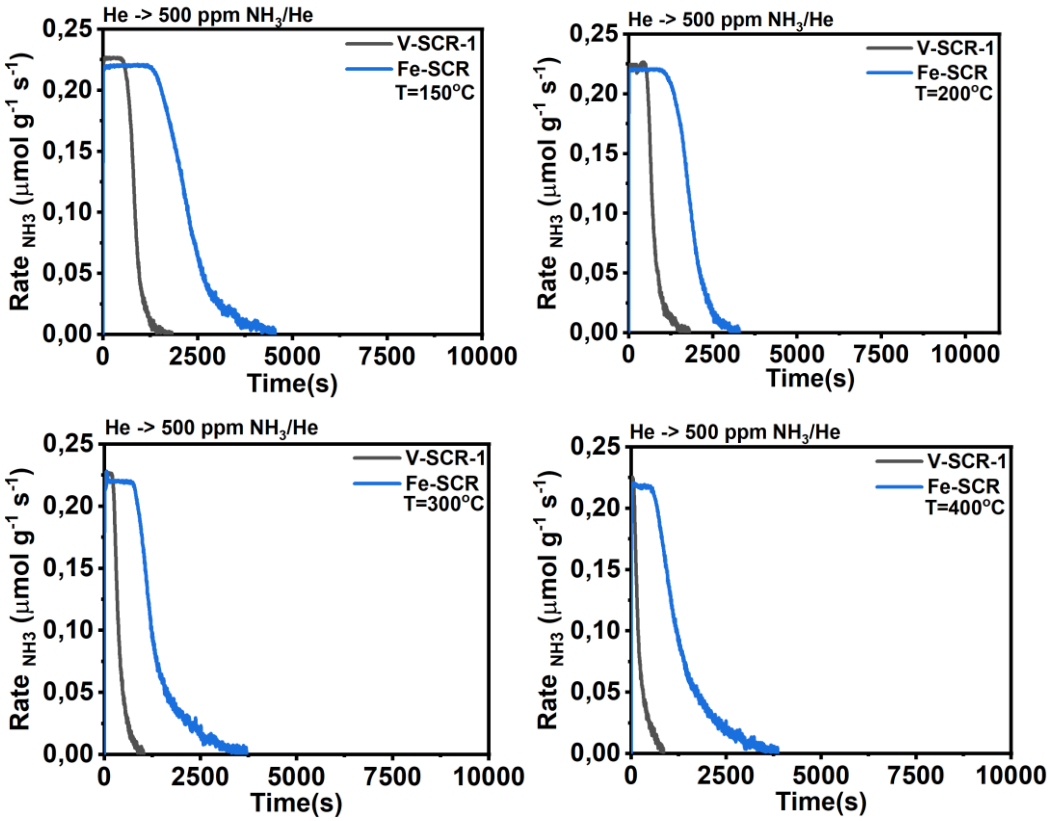


Figure 10. Comparisons of transient rates (µmol g_{sample}^{-1} s^{-1}) of NH_3 adsorption at constant temperature (T= 150, 200, 300 and 400 ºC) on V-SCR-1, and Fe-SCR catalysts (NH_3 feed concentration of 500 ppm).

In the case of isothermal desorption of ammonia in He gas flow, V-SCR-1 presented practically very similar isothermal desorption dynamic rate profiles at the varying temperatures (Fig. 11). This behaviour suggests that the weak adsorption sites populated by ammonia present very similar desorption kinetics in the observed temperatures. In the case of Fe-SCR, the shape of the dynamic rate of ammonia desorption is very similar to that for the V-SCR catalysts but presents higher rates. This result implies similar desorption kinetics from a larger concentration of sites of weak ammonia chemisorption characteristics.

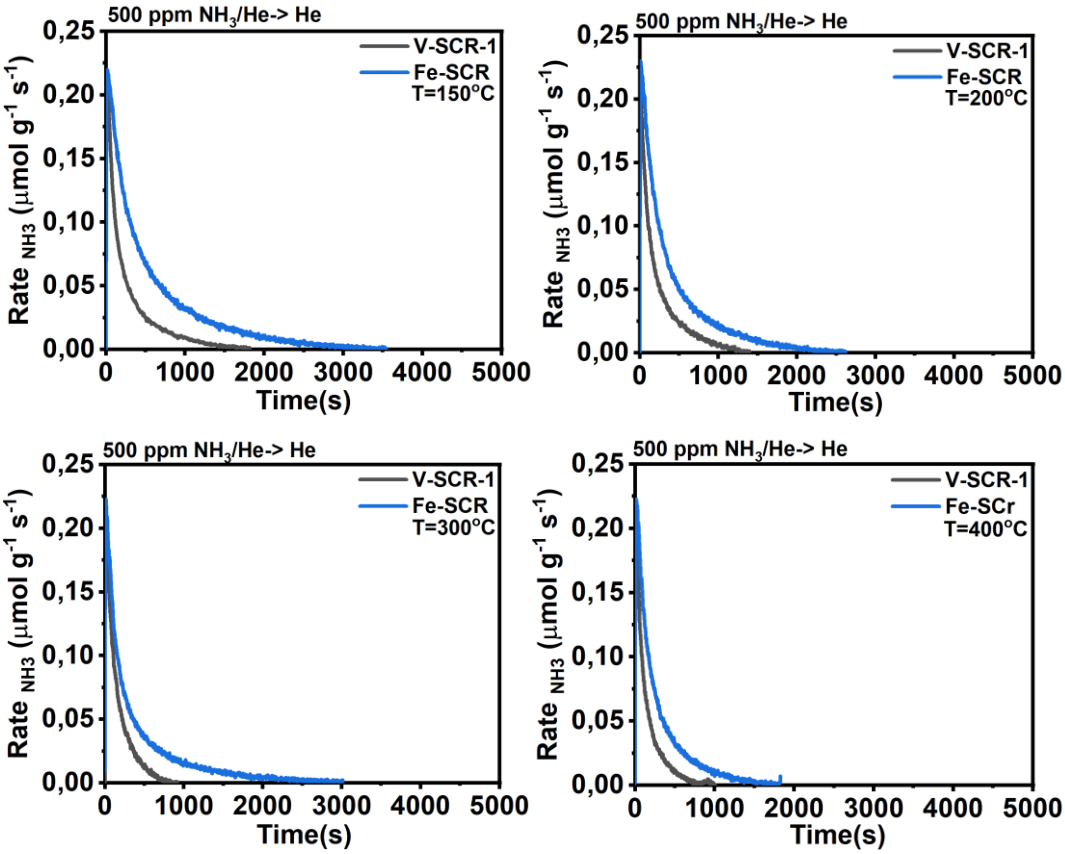


Figure 11. Comparisons of transient rates of isothermal NH_3 desorption in He gas flow at constant temperature T (150, 200, 300 and 400 ºC) on V-SCR-1 and Fe-SCR catalysts.

The temperature-programmed desorption's (TPD) of ammonia are shown in Figure 12 for the 150, 200 and 300 ºC adsorption temperature, respectively over the three SCR catalysts. It should be noted, that where the maximum desorption temperature used for the two V-SCR catalysts was 450 ºC, meanwhile for the Fe-SCR catalyst the temperature was 750 ºC. The desorption rates after the maximum temperature stayed isotherm until the end of the phase.

Based on the shapes of the NH_3-TPD profile as seen in Figure 12, in the case of V-SCR1 and Fe-SCR catalysts, which adsorbed ammonia at 150 ºC, two clearly discernible desorption peaks and shoulders were identified, as opposed to the case of V-SCR-2 catalyst that shows only one broad desorption peak. This result identifies the difference in the strength and kinetics of desorption between the strong type of sites in the two V-SCR catalysts. On the other hand, a comparison of the TPD traces between the V-SCR-1 and Fe-SCR catalysts (Fig. 12) shows a shift of the peak maxima towards higher temperatures for the Fe-SCR, a clear result that the adsorption states of ammonia on Fe-SCR have larger binding strength and activation energy for desorption. The latter catalyst

also presents significantly larger amount of desorbed ammonia under TPD (strong type of adsorption sites) as this is reflected by the larger area under the TPD trace compared to that for the V-SCR-1 catalyst.

As the adsorption temperature increases to 200 ºC (Fig. 11) and 300 ºC, the shape features of the TPD traces change, while the respective amount of ammonia desorption decreases. These results clearly show that the relative population of adsorption sites when the temperature of adsorption increases change. The Fe-SCR remains as the catalyst desorbing the largest amount of ammonia under TPD irrespective of the adsorption temperature.

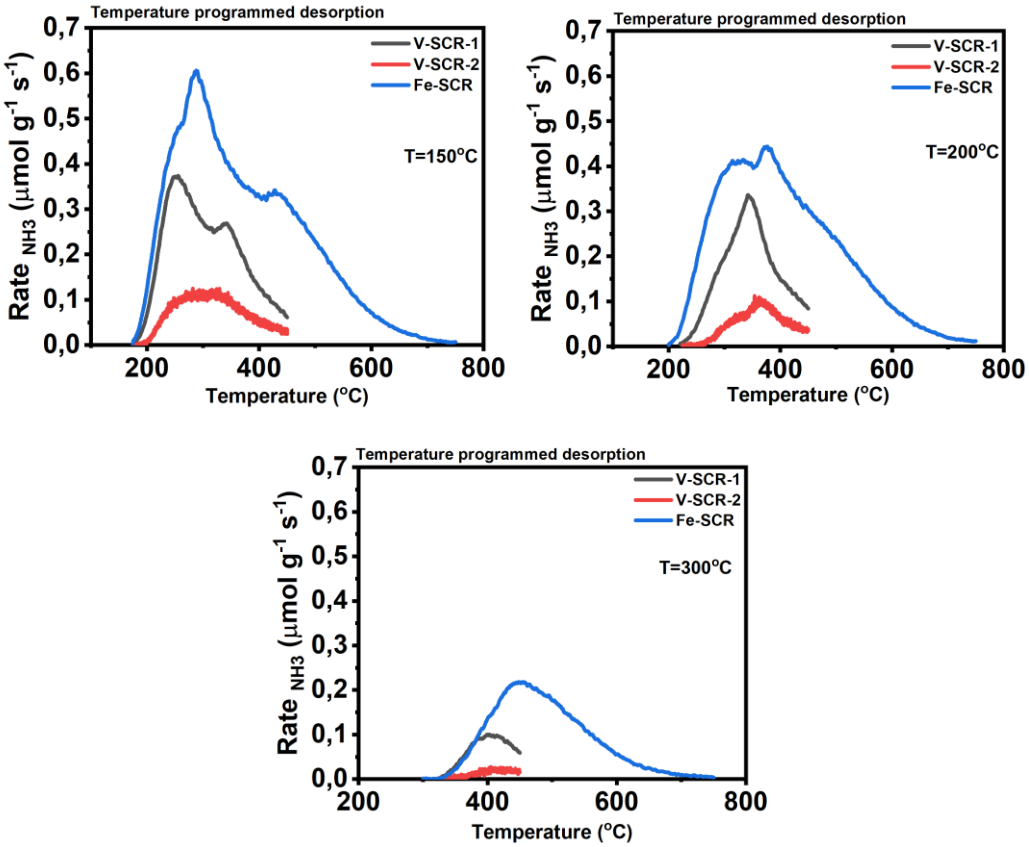


Figure 12. Comparisons of transient rates (µmol g_{sample}^{-1} s^{-1}) of NH_3 desorption during the temperature programmed desorption in He gas flow on the V-SCR-1, V-SCR-2 and Fe-SCR catalysts.

The amount of ammonia adsorbed and desorbed was estimated via the material balances provided in Chapter 5.4.5, and results are depicted in Figure 13 for the four different adsorption temperatures. As mentioned earlier, Fe-SCR is clearly the catalyst with the highest amount of ammonia adsorbed in all temperatures, meanwhile in the case of

isothermal desorption of ammonia, the same trend also repeats. Regarding desorption in TPD, Fe-SCR clearly desorbed the highest amount of ammonia, meanwhile V-SCR-1 and V-SCR-2 had similar results regarding their desorbed amounts.

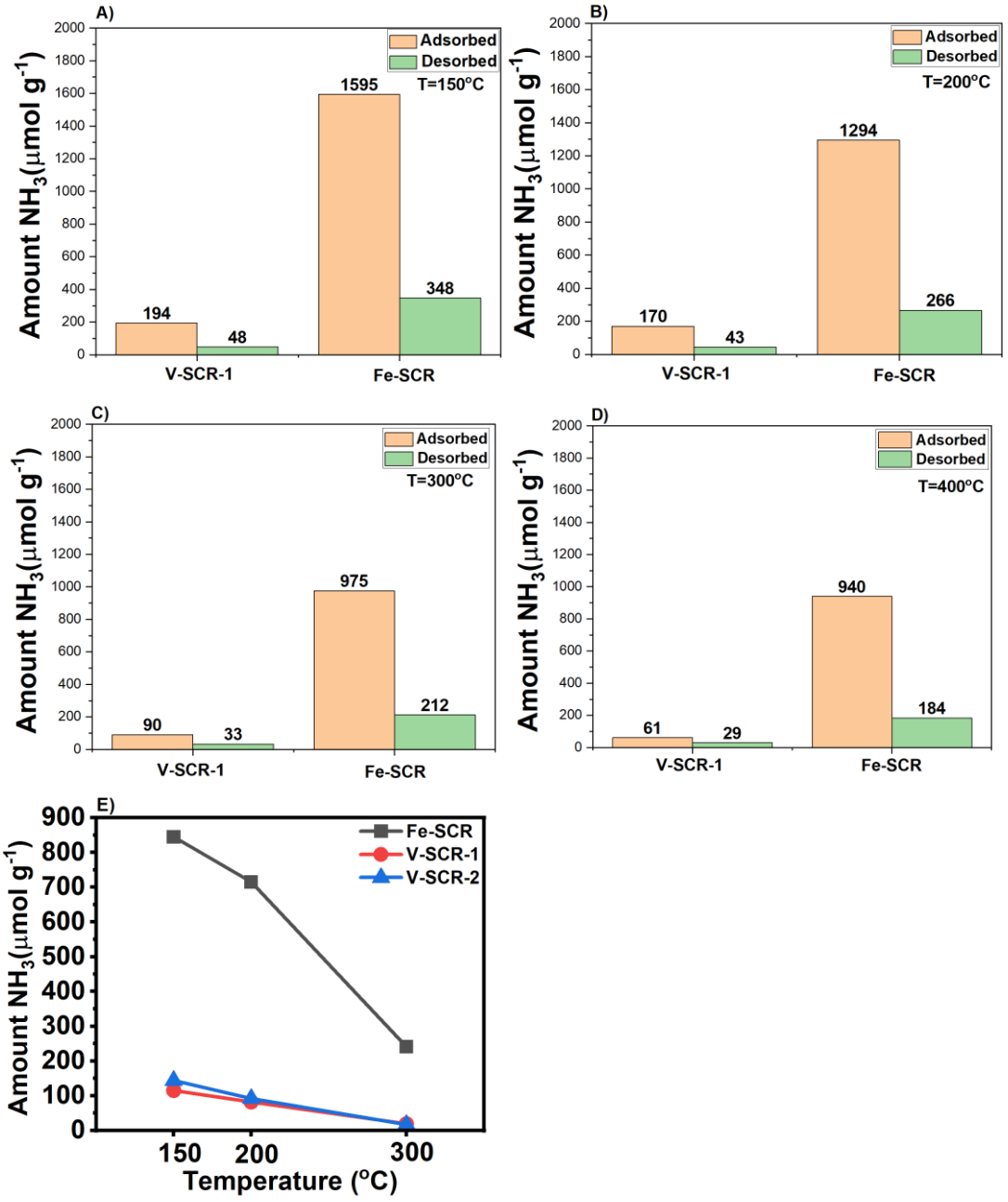


Figure 13. Amount of ammonia (μmol/g catalyst) at A) 150, B) 200, C) 300 and D) 400 °C estimated in the two stages of the NH_3 chemisorption experiments: 1) Isothermal adsorption (He → NH_3/He) and 2) Isothermal desorption (NH_3/He → He). Amount of ammonia desorbed under TPD E) at temperatures 150, 200 and 300 ºC in (He (T_{ads}) → increase T linearly to 450 ºC for V-SCR-1 and V-SCR-2 and 750 ºC for Fe-SCR.

Figure 14A-C compares the effect of adsorption temperature on the transient rate profiles obtained for the V-SCR-1 catalysts in each of the stages of adsorption experiment, namely: adsorption, desorption in He at T and TPD, respectively. As mentioned earlier, the time for which the maximum rate of adsorption occurred (no ammonia at the outlet of reactor) shows a consistent decrease with increasing adsorption temperature, while the time required for full saturation of the catalyst surface decreases with increase of temperature. In the case of isothermal desorption (Fig. 14B), the higher the temperature, the smaller the time for the rate of desorption to reach near zero value and the smaller the amount desorbed (namely the area under the rate curve). However, the differences are smaller than in the case of isothermal adsorption (Fig. 14A). This result suggests that population of weak ammonia adsorption sites decreases to a small extent with temperature than in the case of total adsorption at the same temperature (Fig. 14A).

Figure 14C presents the comparison of the TPD profiles obtained as a function of the various adsorption temperatures applied (150-300 ºC). The TPD done for lowest temperature adsorption (150 ºC) showed both weak and strong adsorption sites (two energetically different adsorption sites. As the adsorption temperature increases, the peak maximum (T_{max}) in the TPD tracer shifts consistently to higher temperature. This is rather the result of the effect of surface coverage of adsorbed species on T_{max} according to the TPD theory (Katada et al., 1997) and less to the population of stronger sites by increasing the adsorption T (activated chemisorption process).

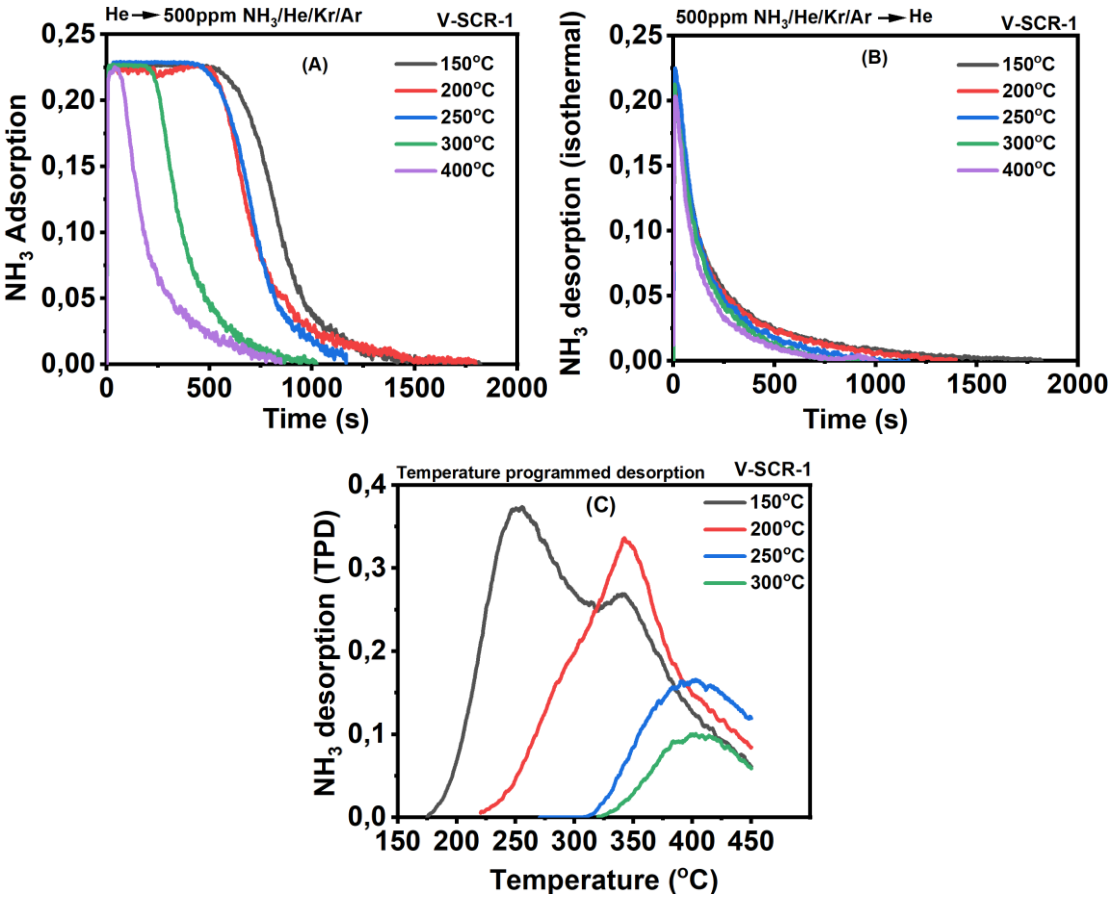


Figure 14. Effect of adsorption temperature on the NH_3 transient adsorption (A), isothermal desorption (B), and TPD (C) rate (μmol g_{sample}^{-1} s^{-1}) profile in the case of V-SCR-1 catalyst (500 ppm NH_3/He adsorption gas mixture, adsorption T: 150, 200, 250 and 300 ºC).

Figure 15 presents corresponding comparative rate results in the case of Fe-SCR catalyst. In general, similar rate profiles with respect to shape were obtained but the time required to reach close to zero rates was significantly larger compared to the case of V-SCR-1. For example, in the case of V-SCR-1, the rate approaches zero values around 800-1800 s, while for the Fe-SCR catalyst ~3000-4000 s. The isothermal desorption profiles had also similar features in shape to those of V-SCR-1, although they appeared slightly less cohesive. The TPD rate profiles for Fe-SCR (Fig. 15C) show a clearly different shape and behaviour when compared to the corresponding V-SCR-1 catalyst. Two desorption peak maxima were observed for the 150 and 200 ºC curves, whereas a single peak for 300 ºC. In the 400 ºC curve there were almost no observable peaks.

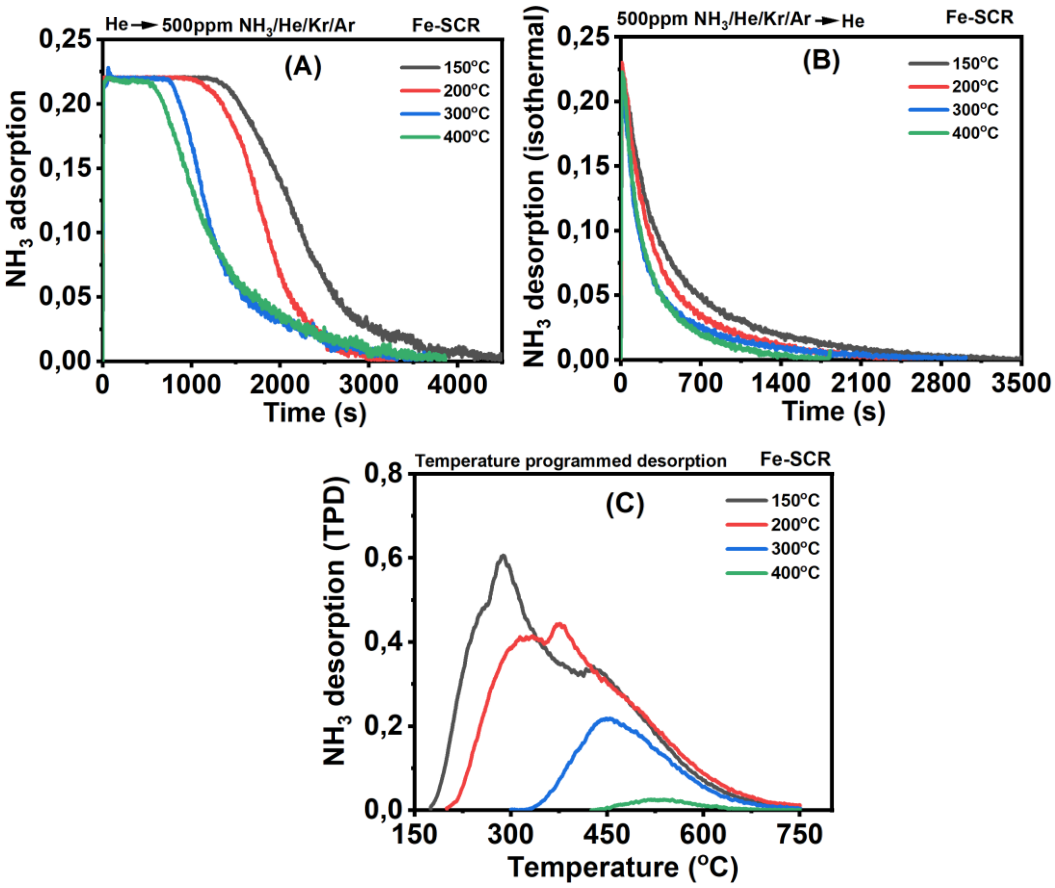


Figure 15. Effect of adsorption temperature on the NH_3 transient adsorption (A), isothermal desorption (B), and TPD (C) rate (μmol g_{sample}^{-1} s^{-1}) profile in the case of Fe-SCR catalyst (500 ppm NH_3/He adsorption gas mixture, adsorption T: 150, 200, 300 and 400 ºC).

6.2.2 Effect of ammonia concentration

The effect of ammonia feed concentration on the adsorbed and desorbed rates of NH_3 and the corresponding amounts (μmol/g) as well as on the TPD traces and amounts are presented and compared in Figures 16, 17 and 18, respectively, for the V-SCR-1 catalyst and for the adsorption temperatures of 150 ºC, 200 ºC, 300 ºC and 400 ºC. The dynamic rates of adsorption (Fig. 16) follow a consistent trend, where they decrease with decreasing ammonia concentration in the feed stream independent of adsorption T. This implies a positive order in the description of kinetics of ammonia adsorption (Rate = k P_{NH3}^{x}; in where x is the order of adsorption).

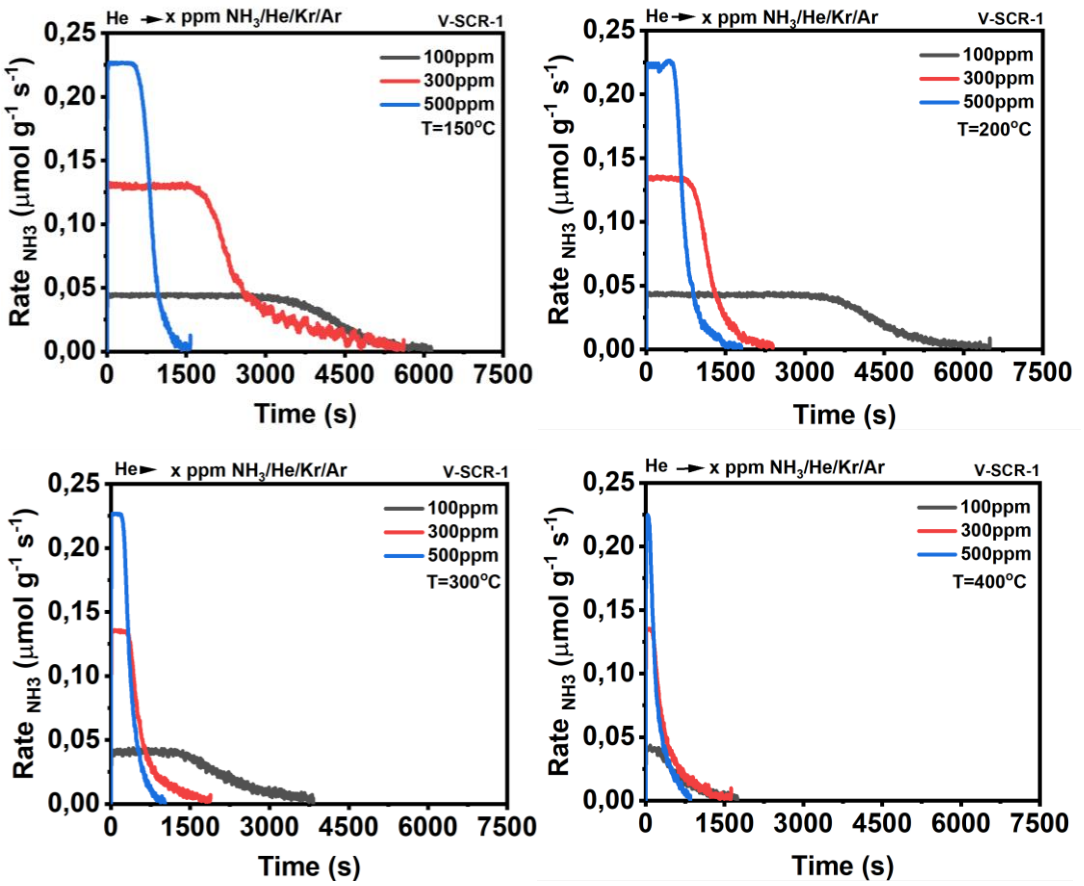


Figure 16. Comparison of NH_3 dynamic adsorption rates (µmol g_{sample}^{-1} s^{-1}) on the V-SCR-1 catalyst as a function of ammonia feed concentration (500, 300 and 100 ppm) and adsorption at 150, 200, 300 and 400 ºC.

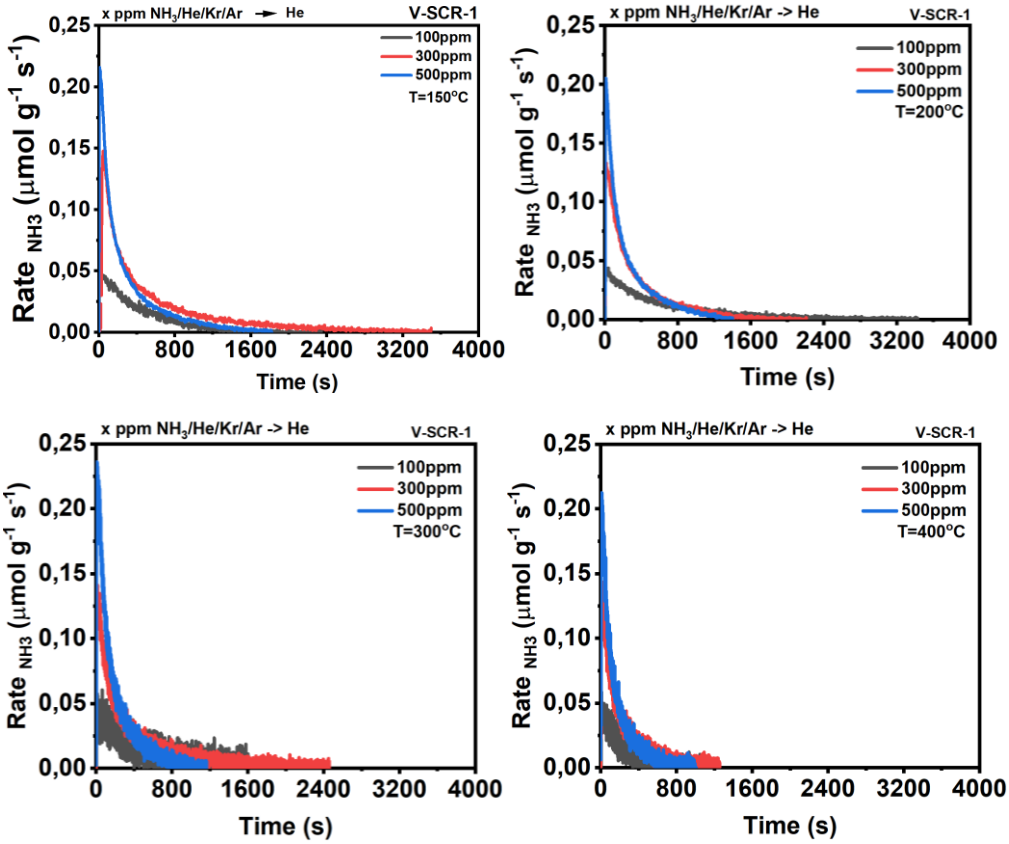


Figure 17. Comparison of isothermal dynamic rates (µmol g_{sample}^{-1} s^{-1}) of NH_3 desorption on the V-SCR-1 catalyst as a function of ammonia feed concentration (500, 300 and 100 ppm) and adsorption T; T=150 ºC, T= 200 ºC, T=300 ºC, and T=400 ºC.

As seen in Figure 17, practically all ammonia desorbed isothermally is obtained at the near same time independent of ammonia concentration in the feed for all adsorption temperatures.

Figure 18 presents the amounts of ammonia adsorbed and desorbed in all three stages of the adsorption experiment for the four-adsorption temperatures investigated for the V-SCR-1 catalyst. For the adsorption temperatures of 150, 200 and 300 ºC, the adsorption amount was found practically independent of ammonia feed concentration, an important result that highlights that all possible adsorption sites are saturated to the same extent independent of the concentration of ammonia in the feed stream. Worthy to note however, that the time required varies as illustrated in Figure 16.

In the case of desorbed ammonia in the TPD stage, for the lowest adsorption T of 150 ºC (Fig. 18), the largest desorbed amount was found to be in the case of using 100 ppm

ammonia in the feed, while for higher adsorption temperatures, similar amounts were found (Fig. 18).

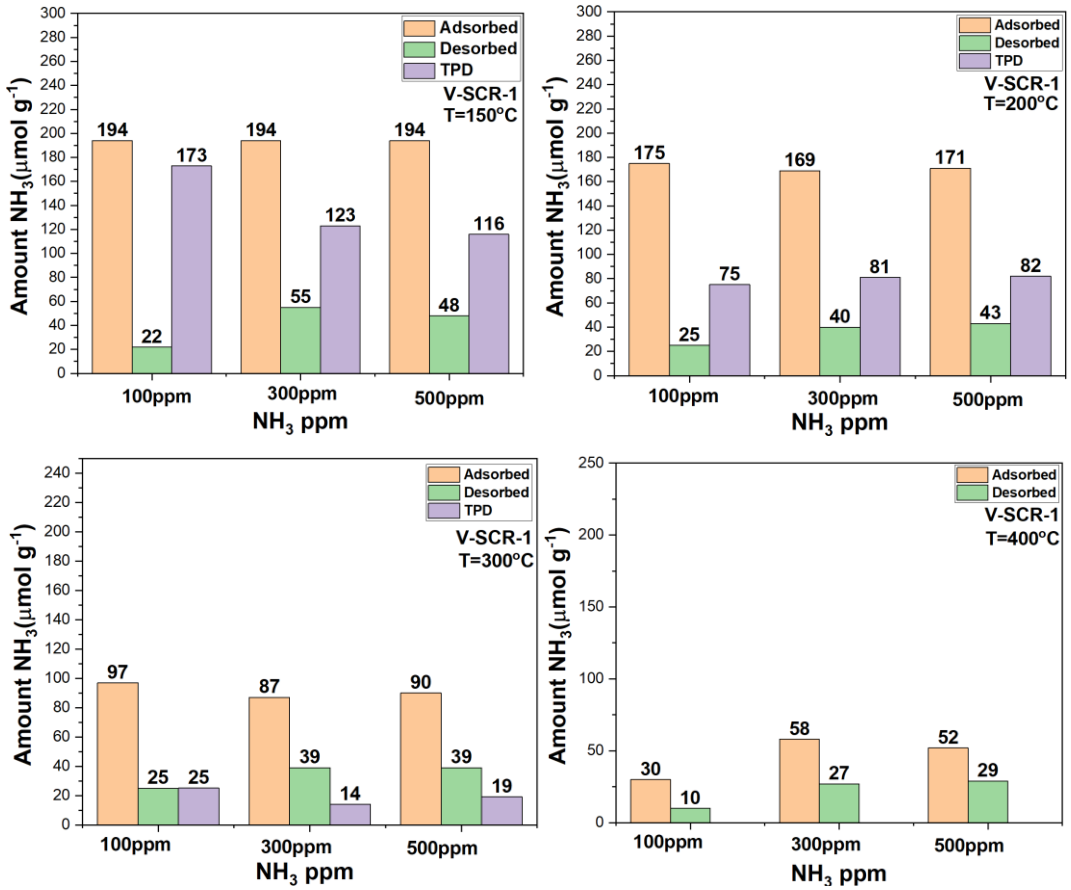


Figure 18. Amounts (μmol/g catalyst) of adsorbed, isothermally desorbed and under TPD. NH_3 at 150, 200, 300 and 400 °C on the V-SCR-1 catalyst.

Figure 19 presents normalized adsorption rate results via the parameter $Z_R = R(t=0/R(t_f)$, where t=0 refers to the initial time where maximum rate is observed, and t_f is the final time the rate was recorded and which has practically a very low value in the case of V-SCR-1 catalyst and as a function of adsorption temperature (Fig. 19). This means that Z_R takes values between unity and zero. These presentations using the Z_R parameter helps to see more clearly the kinetic features of this dynamic adsorption process of ammonia. At the lowest T of adsorption (ca. 150 ºC) and using the largest feed concentration of 500 ppm (Fig. 19), adsorption process is completed much faster than at higher adsorption temperatures. Also, in the case of 300 ppm NH_3 in the feed, distinct two kinds of adsorption processes occur given the change of the slope of Z_R (dZR/dt) with time. This

appears also similar for the lowest feed concentration of 100 ppm ammonia. The increase of adsorption temperature to 200-400 °C (Fig. 19) clearly illustrates the change in the behaviour of Z_R. At the highest temperature of 400 ºC, the kinetics appear very similar (similar Z_R shape curve). Similar results were found for the transient isothermal ammonia desorption stage (Fig. 20).

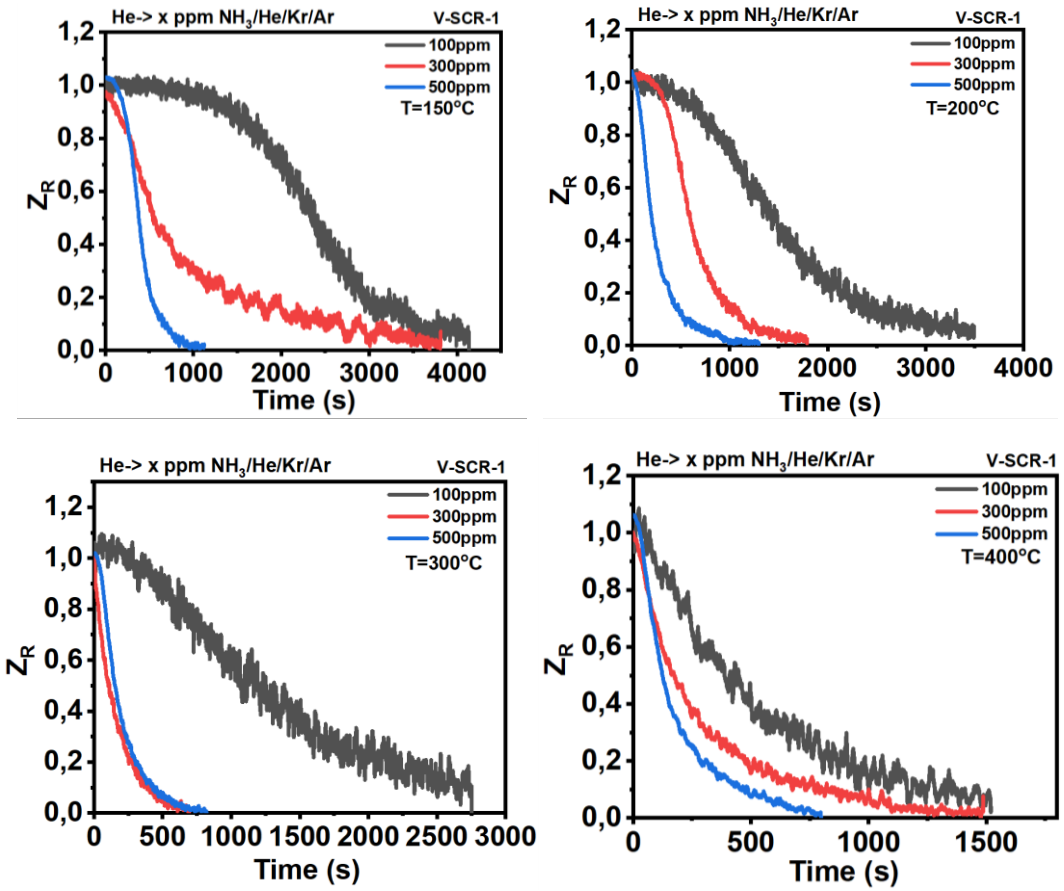


Figure 19. Normalized transient rate (Z_R) of NH_3 adsorption for the V-SCR-1 catalyst at 150, 200, 300 and 400 °C as a function of ammonia concentration in the feed.

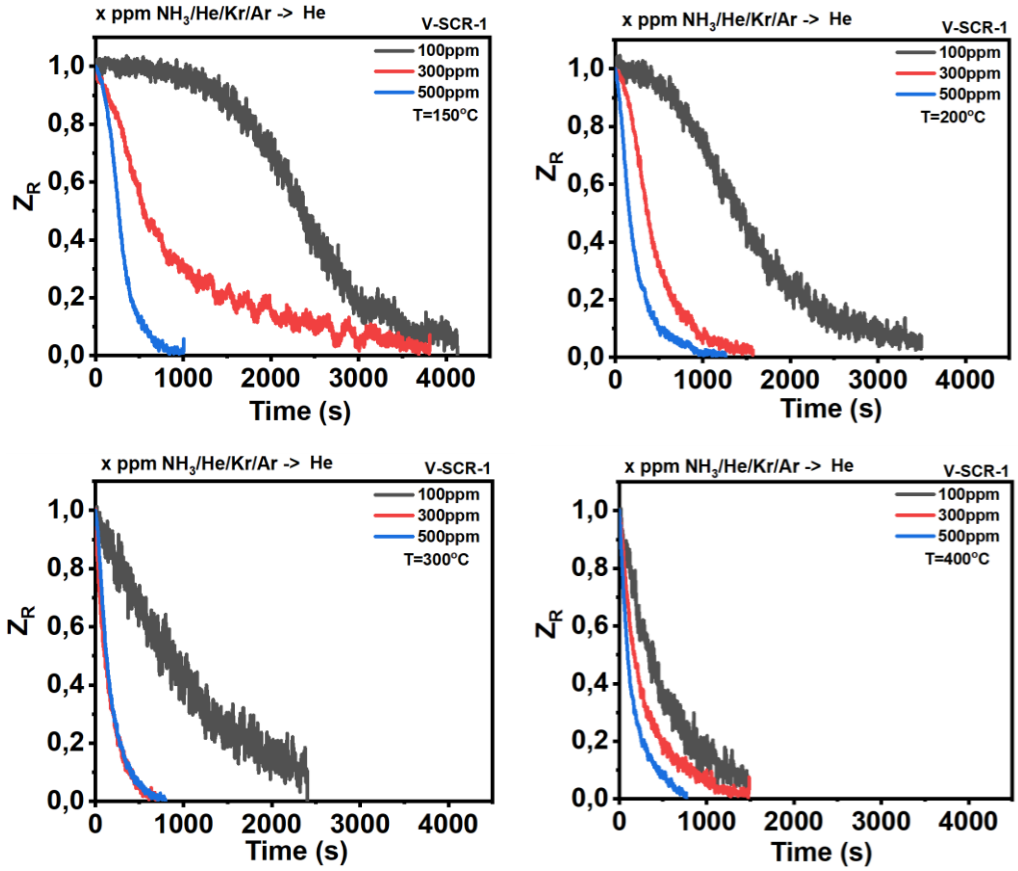


Figure 20. Normalized transient rates (Z_R) of isothermal desorption for the V-SCR-1 at 150, 200, 300 and 400°C.

In the case of Fe-SCR catalyst, Figures 21 and 22 describe corresponding results of Z_R for the adsorption and isothermal desorption stage of the experiment over the V-SCR-1 catalytic system. It can be suggested that practically, there is no or very small effect of ammonia feed concentration in the 300-500 ppm range on the isothermal adsorption and desorption kinetics in all adsorption temperatures (150-400 ºC).

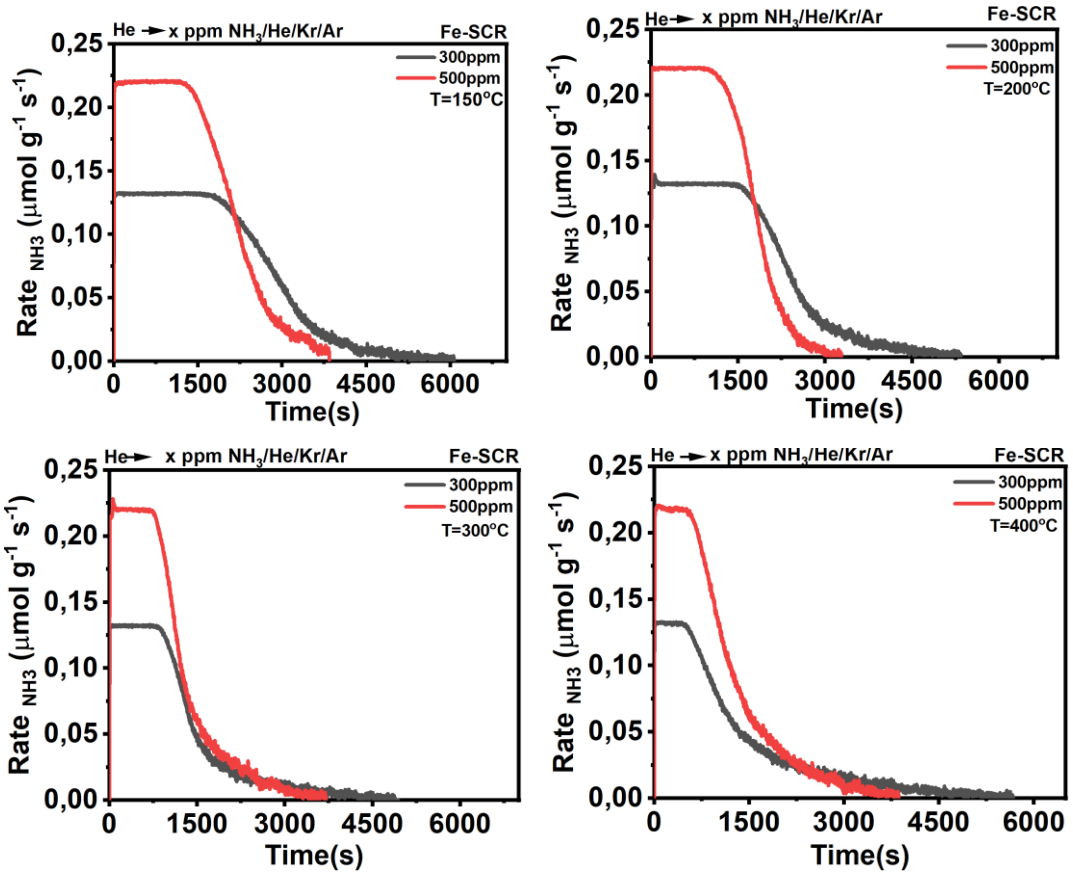


Figure 21. Transient rate of NH_3 adsorption for the Fe-SCR catalyst at 150, 200, 300 and 400 °C as a function of ammonia concentration in the feed.

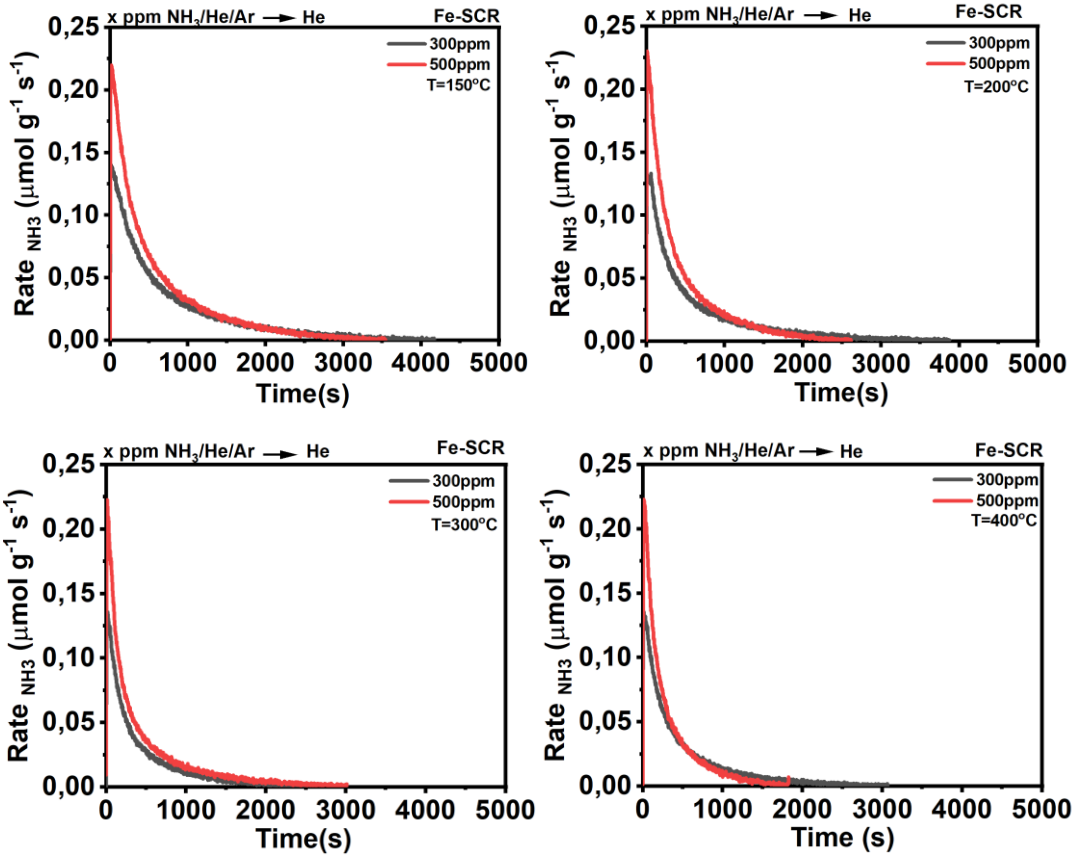


Figure 22. Transient rate of NH_3 isothermal desorption for the Fe-SCR catalyst at 150, 200, 300 and 400 °C as a function of ammonia concentration in the feed.

Figure 23 provides the amounts of ammonia estimated during isothermal adsorption until saturation (A), during isothermal desorption (B) and during TPD (C) as a function of temperature (150-400 °C) for both 300 and 500 ppm NH_3 in the adsorption gas mixture over the Fe-SCR catalyst. There is a clear trend for reduction in the amount of adsorbed ammonia with increasing adsorption temperature for both feed compositions of ammonia (Fig. 23A). The same result was obtained for ammonia desorbed isothermally (Fig. 23B) and during TPD (Fig. 23C).

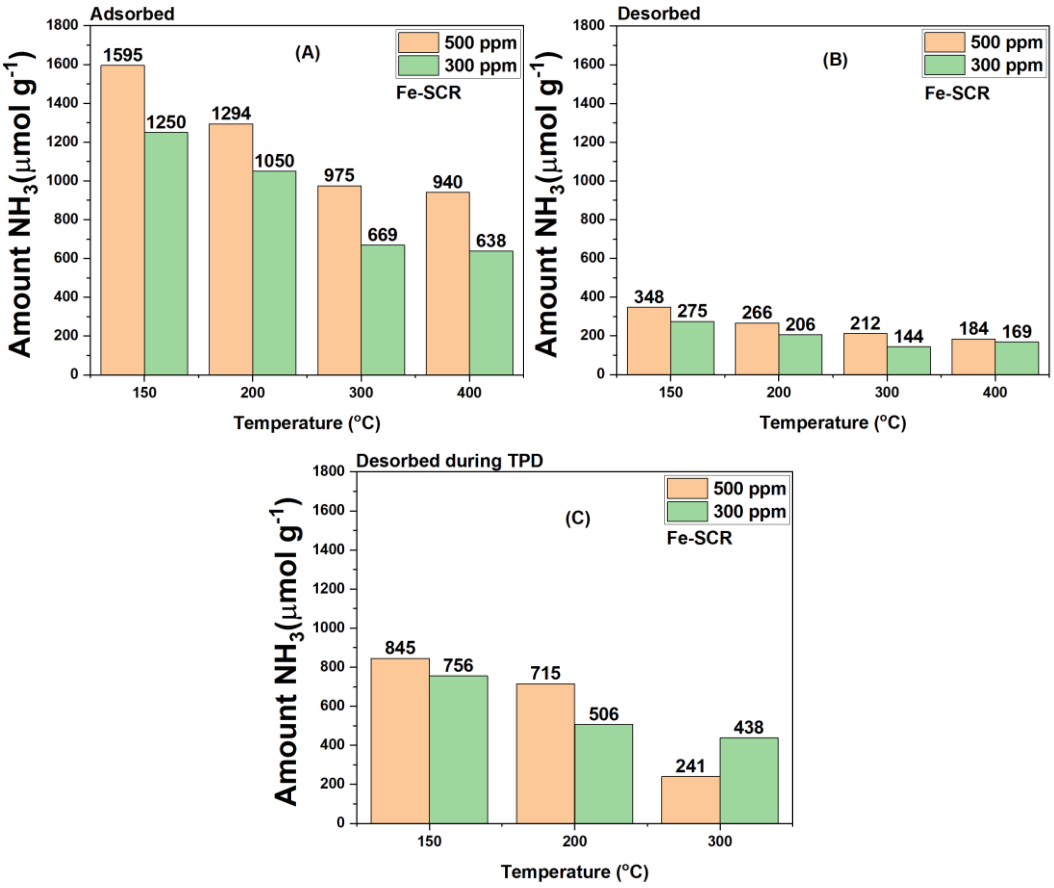


Figure 23. Amounts (μmol/g catalyst) of NH_3 adsorbed until saturation (A) and desorbed in He flow isothermally as a function of adsorption temperature (B), as well as the amounts of ammonia desorbed during TPD following isothermal adsorption and desorption (C) at 150, 200 and 300 ºC for the Fe-SCR catalyst.

Normalized rates Z_R for the isothermal adsorption and desorption stages of the experiment on the Fe-SCR catalyst are presented in Figure 24 and Figure 25, respectively. Practically there is no effect of ammonia feed composition in the 300-500 ppm range for all the adsorption temperatures investigated (150-400 ºC). It appears that the dynamics of adsorption/desorption of ammonia over the Fe-SCR catalyst is not dependent on the concentration of ammonia in the feed (300-500 ppm).

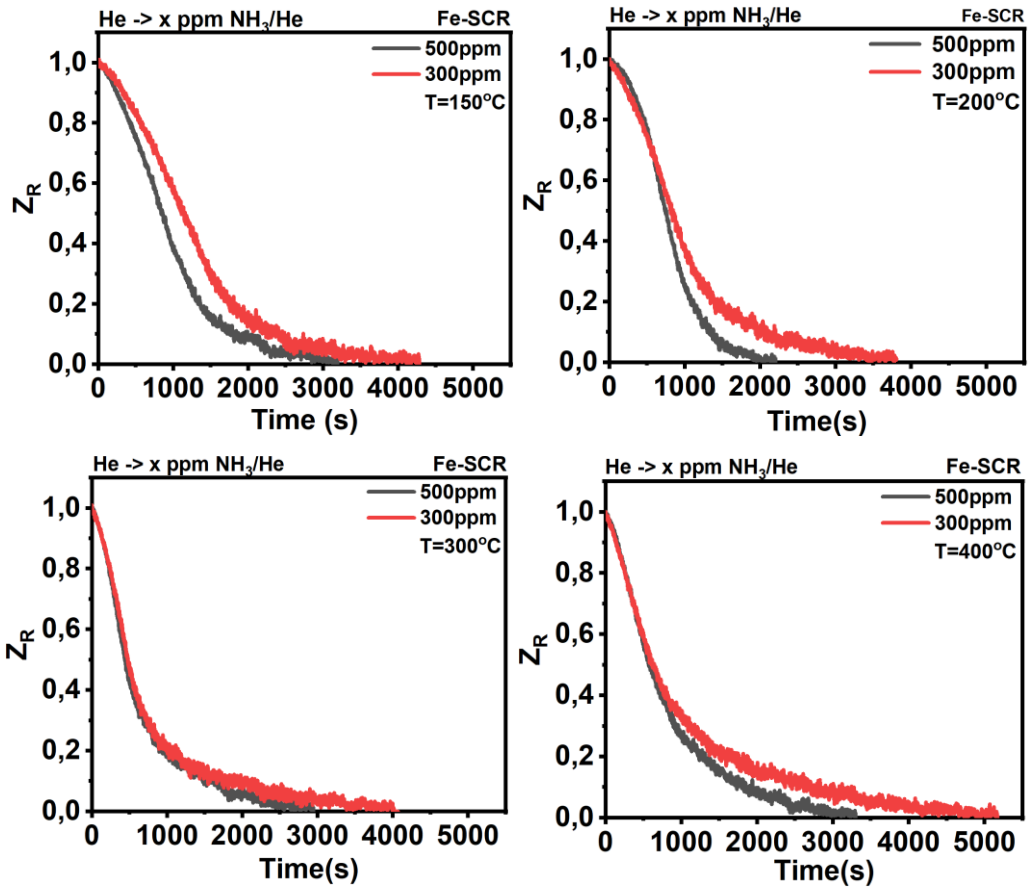


Figure 24. Normalized rates (Z_R) of NH_3 adsorption on Fe-SCR at 150, 200, 300 and 400 °C after using 300 ppm or 500 ppm NH_3 in the adsorption gas mixture.

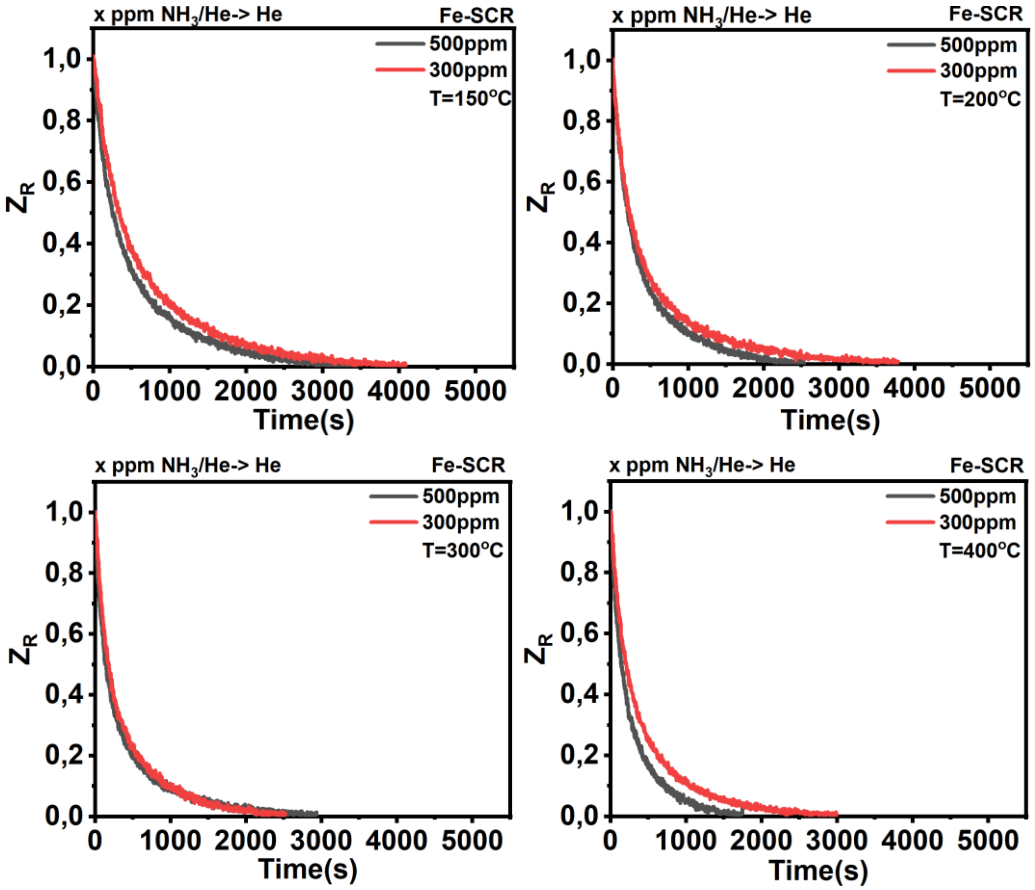


Figure 25. Normalized rates (Z_R) of NH_3 desorption isothermally at 150, 200, 300 and 400 °C on the Fe-SCR after using 300 ppm or 500 ppm NH_3 in the adsorption gas mixture.

6.2.3 Effect of catalyst composition

Figure 26 compares the transient adsorption response of ammonia (500 ppm in the feed) behaviour at 200 ºC in terms of the concentration measured at the outlet of the micro-reactor over the three catalysts investigated. The following remarks are noted.

The V-SCR-1 catalyst exhibit the smallest delay in the appearance of ammonia concentration. This has to do with the strength of adsorption and the amount of sites that strongly adsorb ammonia. Catalysts with the same strength of adsorption but different concentration of surface sites for adsorption will show similar shapes but different times for completion until saturation; at saturation the concentration measured at the outlet of reactor is the same as that in the feed stream.

Fe-SCR shows larger delay until ammonia is seen at the outlet of reactor and a sharp increase towards its saturation state (same value as the feed). This suggests stronger adsorption than that exhibited by the V-SCR1 catalyst.

Pt-DOC shows an initial relatively fast adsorption step, while for longer times the adsorption kinetics seems to become slower and continues for longer times compared to all the other catalysts. To explain this response, we must consider that Pt-DOC is an oxidation catalyst consisting of Pt on alumina-based support. When the concentration response of ammonia at the outlet of reactor is lower than that in the feed, the difference can be the ammonia adsorbed on the catalyst or reacted. The fact that after some time the ammonia concentration reached the feed value, this clearly dictates that there is no steady state catalytic reaction taking place. Ammonia can be adsorbed on alumina at 200 ºC (Nova and Tronconi, 2014). and can also decompose on Pt into NH_x-s and H-s species (Imbihl et al., 2007). We speculate that the initial response is due to ammonia adsorption on alumina, while the later slow response to NH_3 dissociation on Pt. The fact that no oxygen is present in the feed, after some time the NH_x-s/H-s species accumulate on the Pt surface and blocks sites for further activation of ammonia, thus the concentration of ammonia at the outlet will reach the feed value.

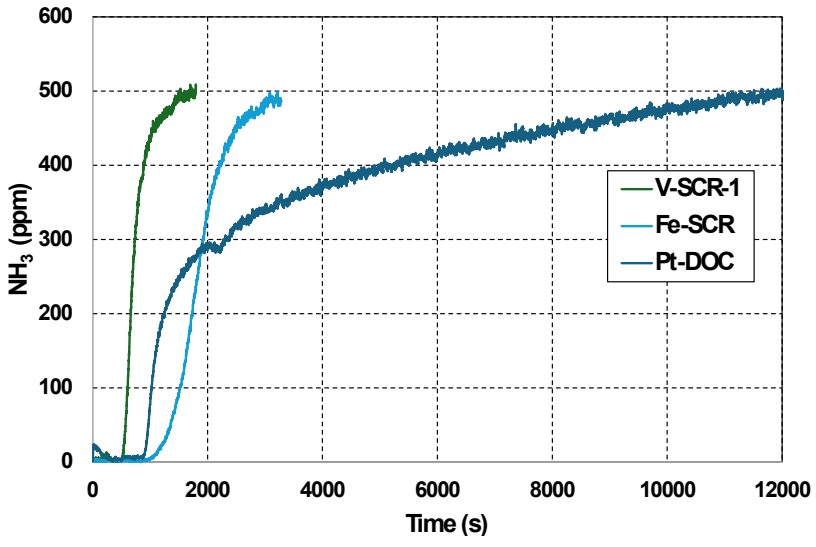


Figure 26. NH_3 concentration in transient adsorption experiments on V-SCR-1, Fe-SCR and Pt-DOC oxidation catalyst at 200 ºC in dry conditions (500 ppm NH_3/He).

6.3 Effect of N_2O on ammonia adsorption/desorption

The presence of N_2O in the adsorption mixture of ammonia is of practical interest for the application of NH_3 as fuel and the aftertreatment of the exhaust/flue gas stream. In the present work we have considered the presence of 50 ppm of N_2O in the NH_3/He feed (adsorption gas, $NH_3/N_2O = 10$) and focused on the Fe-SCR and V-SCR-1 catalysts. The following remarks are noted:

The presence of N_2O in the ammonia adsorption gas mixture influenced only the amount of ammonia adsorption and not the kinetic rate of adsorption based on the shape and position in time of the dynamic rate profiles presented in Figure 27 for the Fe-SCR catalyst. It is clearly shown that the response curve of ammonia gas shifted to lower times when 50 ppm N_2O were present in the adsorption mixture. This effect was similar for the temperatures of 150 and 300 ºC.

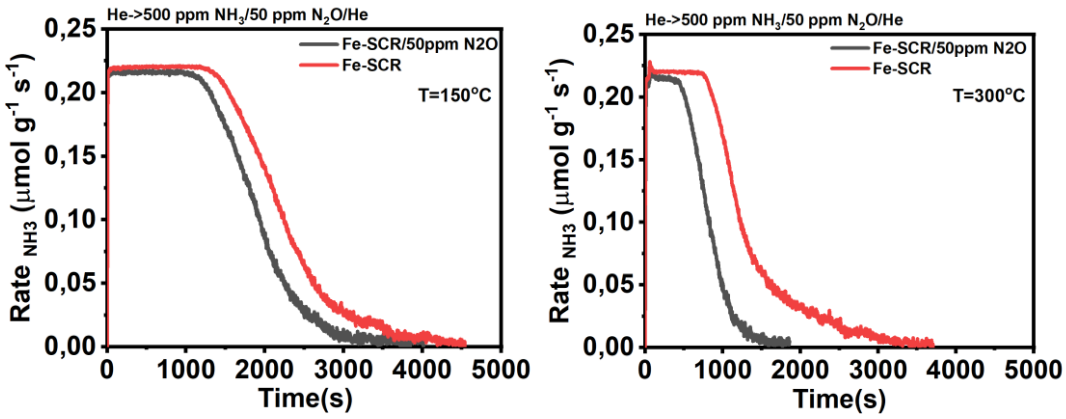


Figure 27. The effect of 50 ppm N_2O in the feed stream on NH_3 dynamic isothermal adsorption rate on the Fe-SCR catalyst at 150 and 300 °C (feed 500 ppm NH_3).

The presence of N_2O in the ammonia adsorption gas had no influence on the ammonia dynamic rate of adsorption and thus on the amount adsorbed in the case of V-SCR-1 catalyst (Fig. 28).

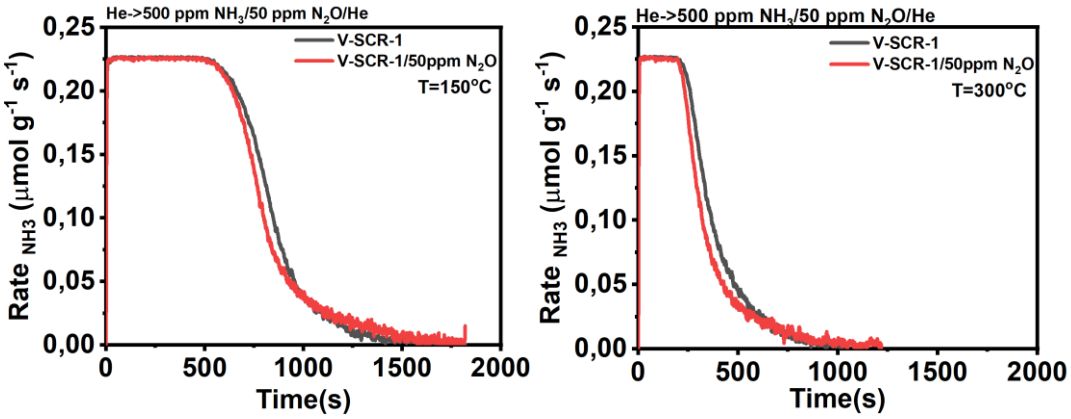


Figure 28. The effect of 50 ppm N_2O in the feed stream on NH_3 dynamic adsorption rate on the V-SCR-1 catalyst at 150 and 300 °C (feed 500 ppm NH_3).

The presence of N_2O in the ammonia adsorption gas influenced slightly the isothermal desorption of ammonia following the adsorption stage of the experiment in the case of V-SCR-1 catalyst (Fig. 29). On the other hand, no effect was seen in the case of Fe-SCR catalyst (Fig. 30).

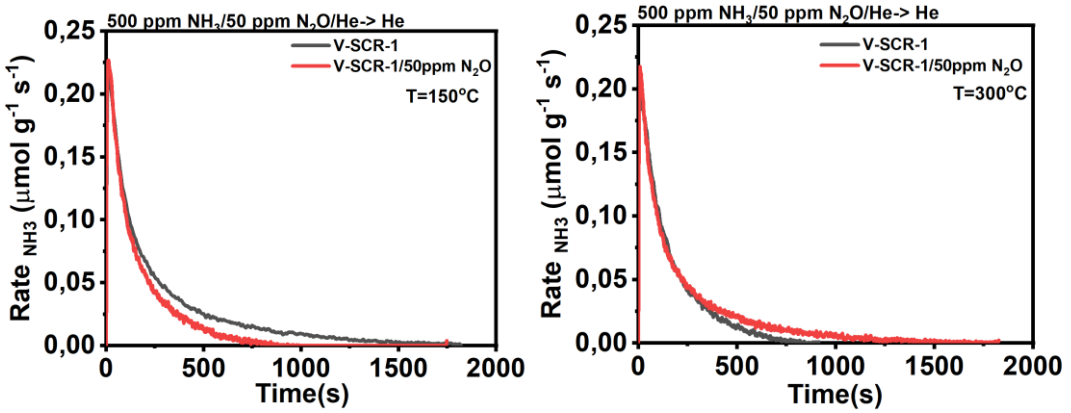


Figure 29. The effect of 50 ppm N_2O in the feed stream on NH_3 dynamic isothermal desorption rate in He flow at 150 and 300 °C on the V-SCR-1 catalyst.

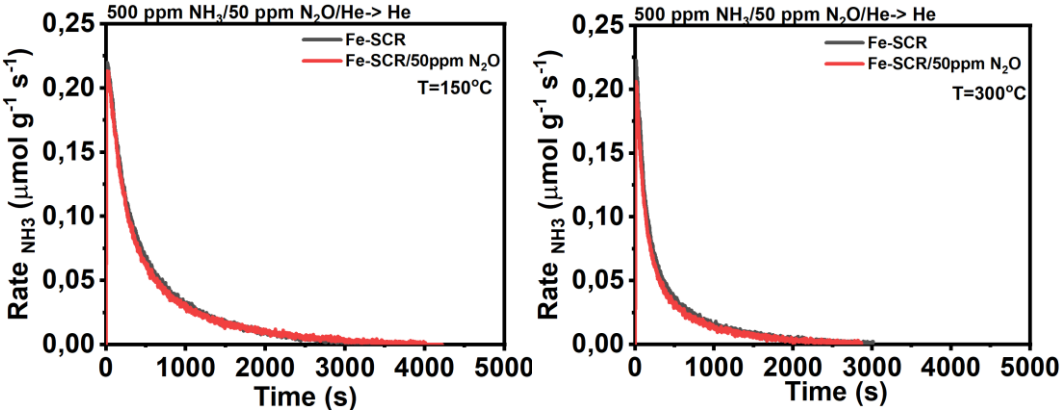


Figure 30. The effect of 50 ppm N_2O in the feed on NH_3 dynamic isothermal desorption rate in He flow at 150 and 300 °C on the Fe-SCR catalyst.

The presence of N_2O in the ammonia adsorption gas had also no effect on the shape and position of TPD traces for the Fe-SCR (Fig. 31) and V-SCR-1 (Fig. 32) catalysts. The only effect clearly seen is the slightly lower amount of strongly bound ammonia desorbed, in excellent agreement with the results obtained during the adsorption stage of the experiment.

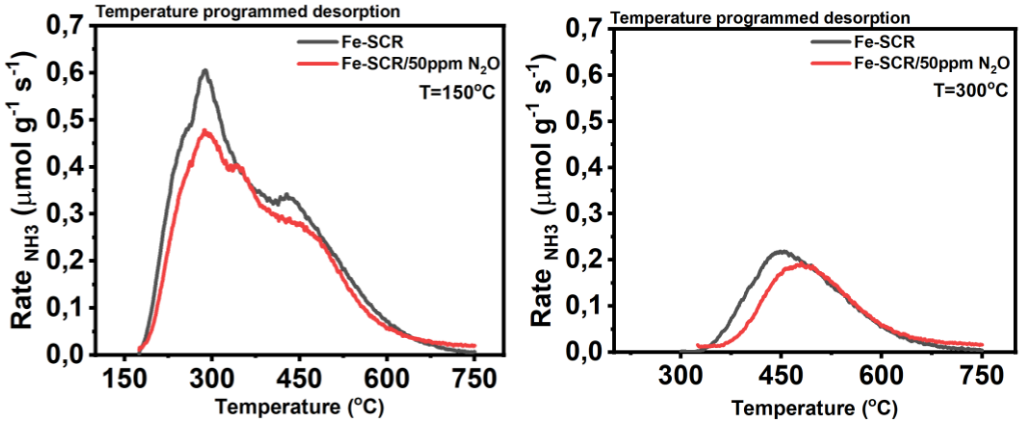


Figure 31. The effect of 50 ppm N_2O in the feed on NH_3 desorption rate in TPD on the Fe-SCR catalyst.

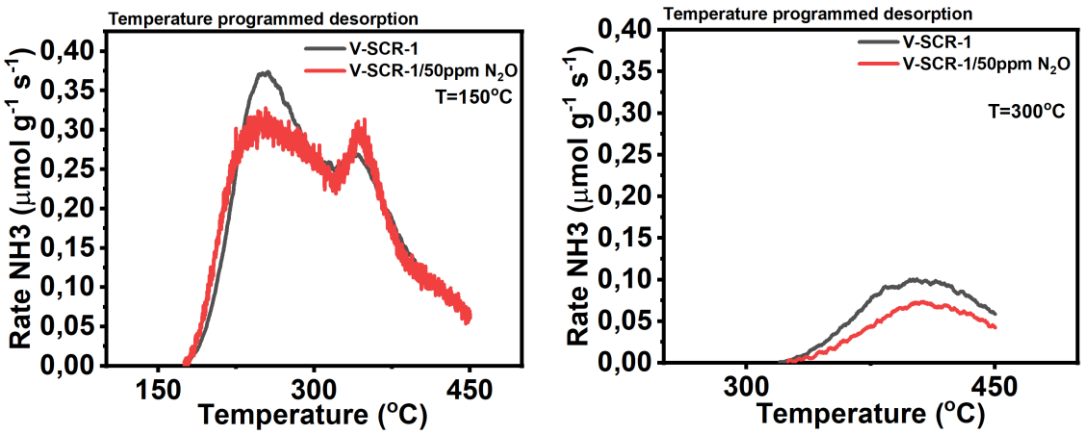


Figure 32. The effect of 50 ppm N_2O in the feed on NH_3 desorption rate in TPD on the V-SCR-1 catalyst.

A comparison of the amounts of ammonia adsorbed/desorbed estimated for the three stages of the adsorption experiment in the presence and absence of N_2O at 150 and 300 ºC is provided in Figure 33 for the V-SCR-1 catalyst and in Figure 34 for the Fe-SCR catalyst.

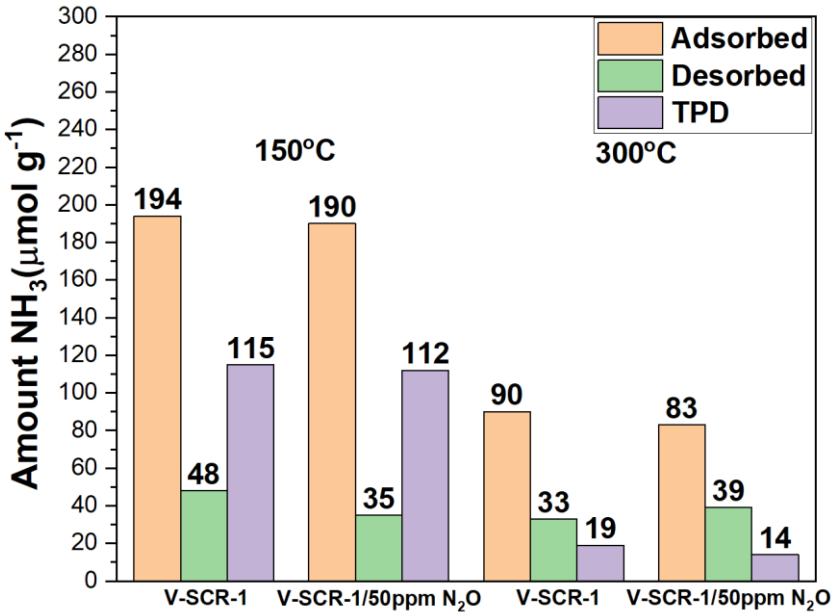


Figure 33. The effect of 50 ppm N_2O on the amounts (µmol/g catalyst) of NH_3 adsorption, isothermal desorption and desorption in heating ramp (TPD) with V-SCR-1 catalyst. at 150 and 300°C.

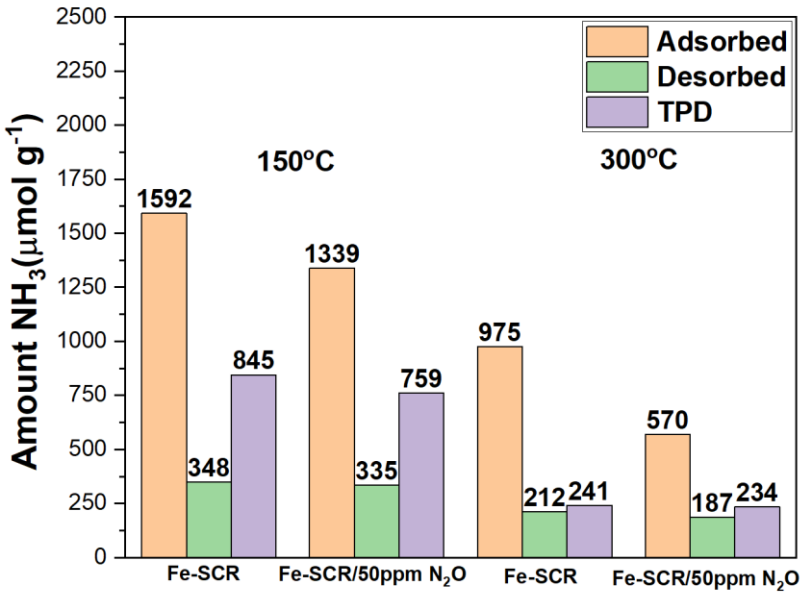


Figure 34. The effect of 50 ppm N_2O and temperature on the amounts (μmol/g catalyst) of NH_3 adsorption, desorption at constant temperature and desorption in heating ramp (TPD) with the Fe-SCR catalyst.

6.4 Ammonia adsorption followed by oxidation (dry conditions)

The reactivity of adsorbed ammonia towards oxidation at 200 ºC was investigated and compared over the Pt-DOC, V-SCR-1, and V-SCR-1/Pt-DOC catalytic systems. The experiment was described in Section 5.4.3. Figure 35 compares the amounts of ammonia adsorbed at 300 ºC before the feed was switched to 5 vol% O_2/He at 300 ºC to study the dynamics of oxidation of pre-adsorbed ammonia with oxygen gas. As explained and discussed previously, in the case of the Pt-DOC catalyst adsorption of ammonia on alumina support and ammonia dissociation on Pt can be both present, which can increase the total adsorption capacity. The dissociative adsorption of ammonia on Pt is given in the following chemical equation:

$$NH_3\,(g) + (4\text{-}x)\,s\,(Pt) \rightarrow NH_x\text{-}s + (3\text{-}x)\,H\text{-}s \qquad (14)$$

No H_2(g) gas was seen during the isothermal adsorption experiment at 300 ºC on the Pt/DOC catalyst.

As seen in Figure 35, Pt/DOC presents the largest amount of adsorbed ammonia, where in this case "adsorbed ammonia" must include the NH_x-s species in addition to the ammonia adsorbed on alumina in a non-dissociated form. However, when the number of experiments was limited in these conditions, additional research could give knowledge.

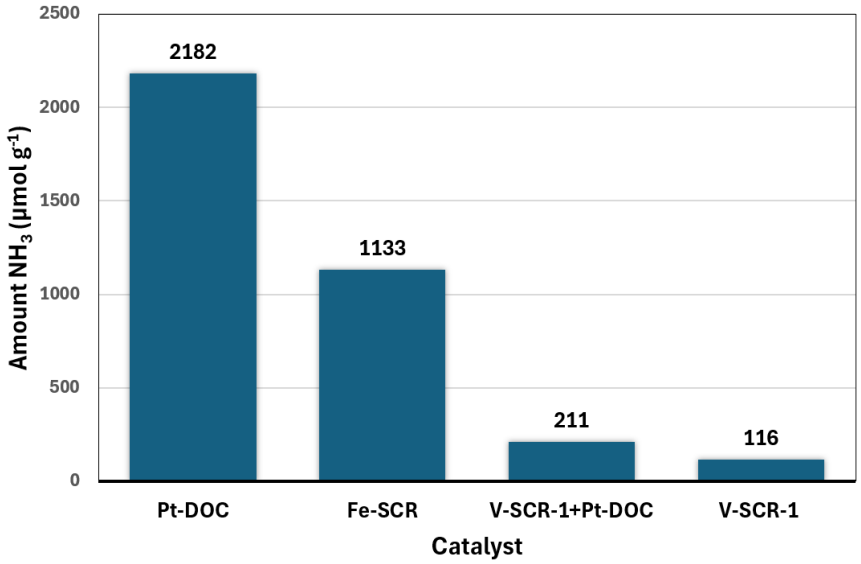


Figure 35. Adsorbed NH_3 (µmol NH_3/g catalyst) on the four SCR catalysts after using 500 ppm NH_3 in the adsorption gas mixture at 300 ºC.

After the adsorption step at 300 ºC with 500 ppm NH_3 in the feed, the flow was changed to 5% O_2 in He at the same temperature of 300 ºC. During this step, pre-adsorbed ammonia species (NH_x-s; x-1-3) could react with oxygen to form various N-containing species (e.g., N_2, NO_2, N_2O) and H_2O, but at the same time some ammonia could desorb without reaction.

Figure 36 shows the amounts of ammonia (NH_3) formed, where the order is similar to that found for the "adsorbed" ammonia (Fig. 35).

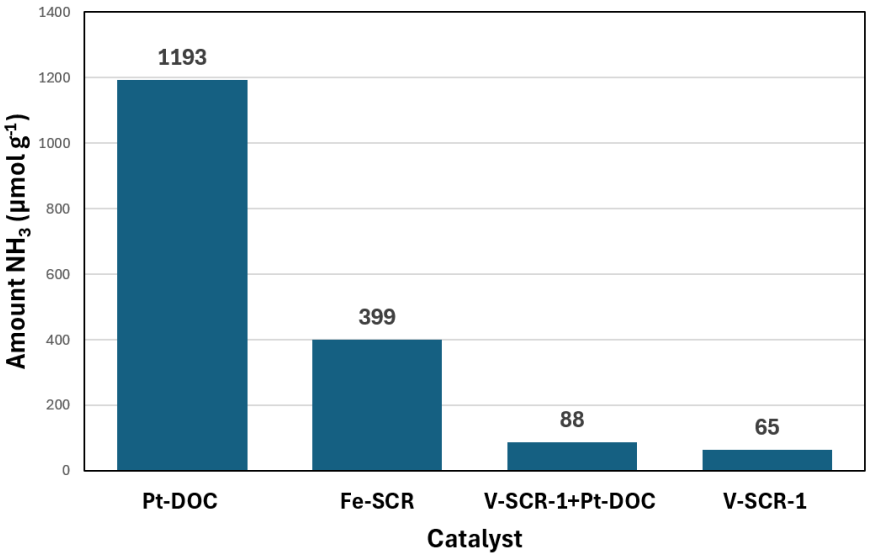


Figure 36. Amount of desorbed NH_3 (µmol/g catalyst) formed during the 5%O_2/He gas switch at 300 ºC, following ammonia treatment of the catalysts at 300 ºC in 500 ppm NH_3/He.

Figure 37 displays the amounts of N_2 formed under the 5%O_2/He gas treatment. It is clearly seen that Pt-DOC showed the largest amount of N_2 formed due to the reaction of preabsorbed NH_x-s with oxygen. Fe-SCR appears to be the catalyst with the 2nd largest amount of N_2 formed, while V-SCR catalysts had very low tendency for N_2 formation. This result was confirmed by catalytic measurements on NH_3/O_2/He reaction.

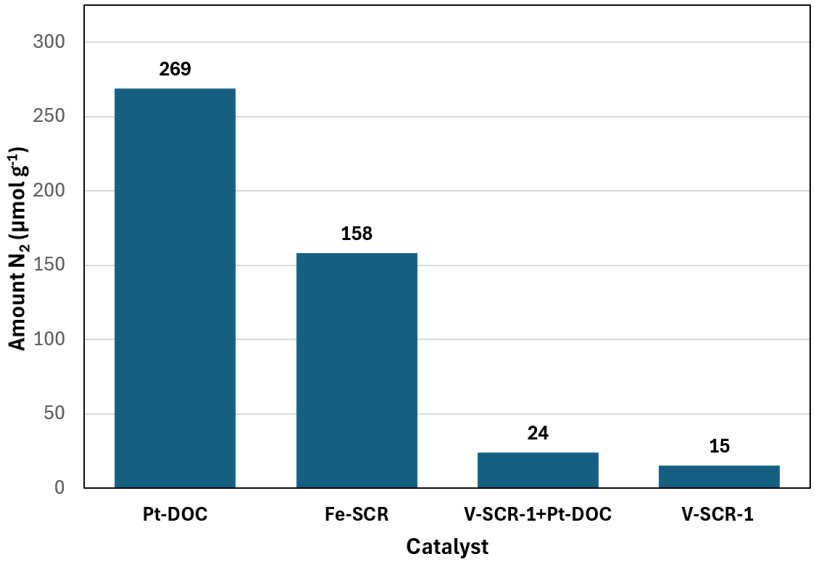


Figure 37. Formed N_2 (µmol/g catalyst) on SCR catalysts in the presence of pre-adsorbed 500 ppm NH_3 at 300°C.

N_2O formation from pre-adsorbed NH_3 was low (Fig. 38). As can be assumed, Pt-DOC and V-SCR1/Pt-DOC had the highest N_2O formation at 300°C. Pt catalysts are known about the tendency to N_2O and NO formation in NH_3 oxidation or SCR reactions (Li et al., 2025). N_2O formation was negligible on the Fe-SCR, V-SCR-1 and catalysts.

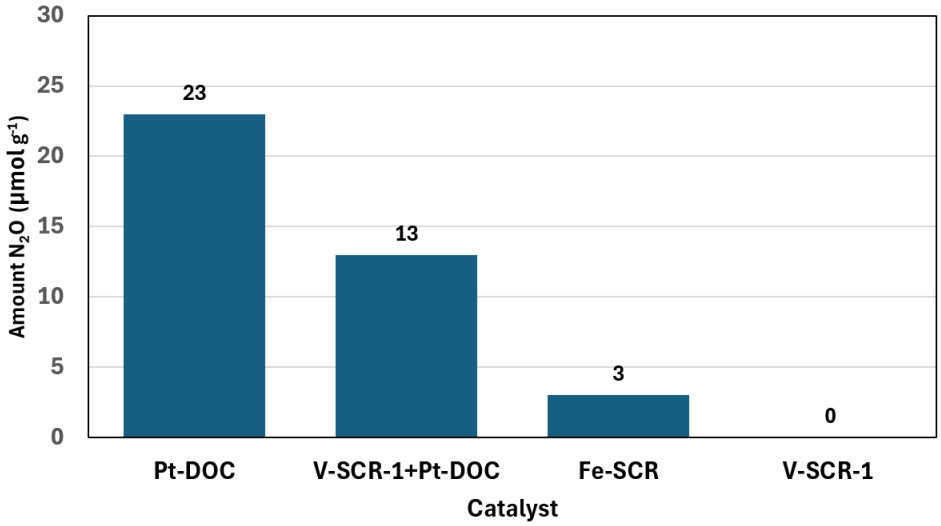


Figure 38. Formed N_2O (µmol/g catalyst) on SCR catalysts in the presence pre-adsorbed 500 ppm NH_3 at 300°C.

On the desorption of NO (30 m/z) there was least variation between the amount when compared to the rest of the side product formations, as seen in Figure 39. The Pt-DOC catalyst had the highest formation of NO by a high margin on both temperatures, meanwhile the other catalysts had significantly lower performances although they were of same magnitude capacity-wise.

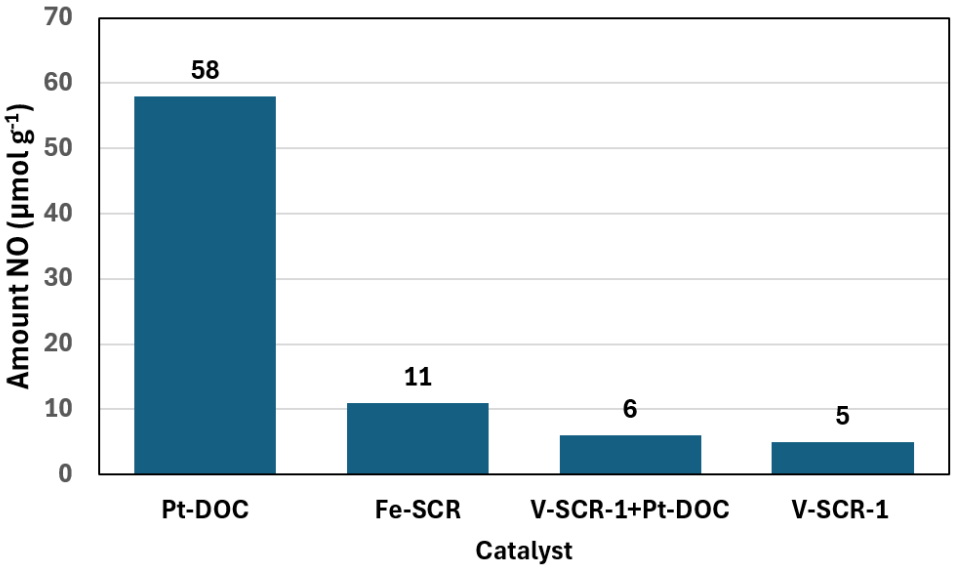


Figure 39. Formed NO (µmol/g catalyst) on SCR catalysts in the presence of pre-adsorbed 500 ppm NH_3 at 300°C.

6.5 Ammonia adsorption on SCR catalysts in wet conditions

On the V-SCR-1, it was clear that 5% H_2O had a positive impact on the adsorption capacity, showing higher adsorption capacities for both 150 ℃ and 300 °C (Fig. 40). Regarding the isothermally desorbed NH_3 5% H_2O resulted in a higher amount at both temperatures as well, NH_3 desorption was higher in the presence of water by TPD at 150 °C but results at 300 °C differed from that trend, when NH_3 desorption was negligible at 300 °C in the presence of water. This can be caused by experimental tolerances with those small concentrations (no repeat test done).

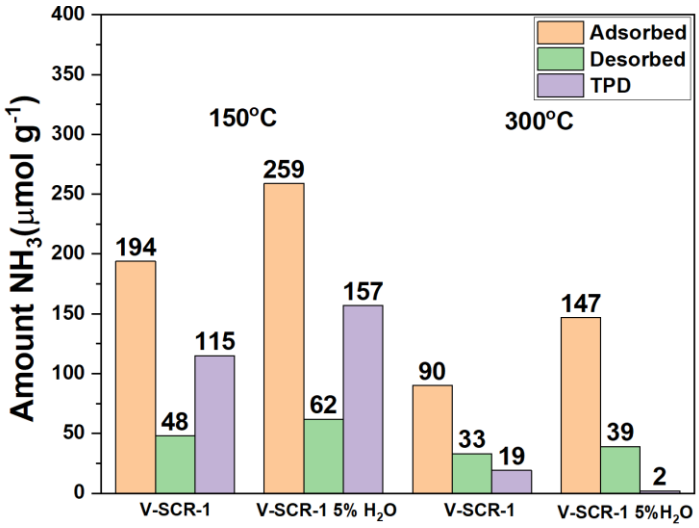


Figure 40. The effect of 5% water on the amounts of NH_3 (μmol/g catalyst) adsorption, isothermal desorption and desorption in heating ramp (TPD) on the V-SCR-1 catalyst.

Presence of 5% H_2O in the NH_3 feed had a negative impact on the adsorption capacity on the Fe-SCR catalyst, at least at 200 °C (Fig. 41). At 300 °C water did not cause any difference in the adsorption capacity. Regarding the isothermal NH_3 desorbed amounts, the effect of water was also seen. At 200 °C, there were also minor differences between isothermally desorbed ammonia, but at 300 °C there was a major drop of adsorption in the presence of 5% H_2O. At 200 °C a larger drop of strongly bound NH_3 (TPD) was detected due to the presence of 5% water. On the Fe-SCR there seems to be major hindering effects by water regarding ammonia adsorption, especially in lower temperature ranges such as 200 °C.

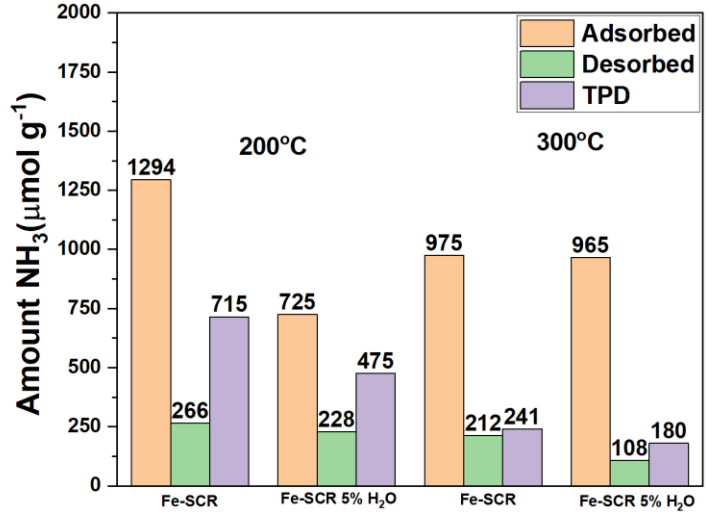


Figure 41. The effect of 5% water on the amounts of NH_3 (μmol/g catalyst) adsorption, desorption at isothermal desorption in heating ramp (TPD) on the Fe-SCR catalyst.

Regarding the adsorption rates as seen in Figure 42 and 43, there are notable differences. On the V-SCR-1 there are major differences in the adsorption behaviour at both temperatures. When compared with the dry NH_3 adsorption, in NH_3 adsorption feed with 5% H_2O begins in a similar adsorption pattern at the beginning, but rate fell a lot slower and with a longer, wavelike curve. On the Fe-SCR catalyst, the stable adsorption period was shorter and steeper at 200 °C, and at 300 °C it is similarly shorter, but with a longer wavelike curve like the V-SCR-1. The rates were more oscillating with 5% H_2O which can be explained by the presence of the water which affects the MS analysis responses.

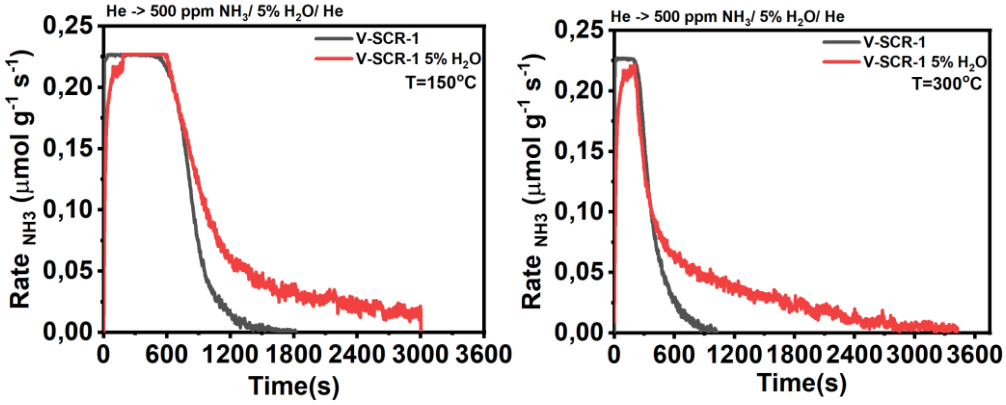


Figure 42. The effect of 5% water on the NH_3 adsorption rate (µmol/g catalyst) at 150 °C and 300 °C on the V-SCR-1 catalyst.

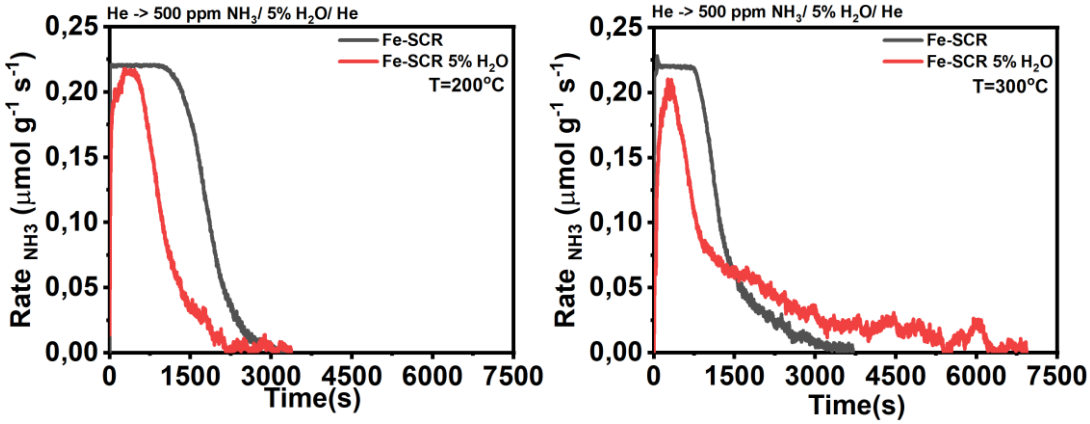


Figure 43. The effect of 5% water on the NH_3 adsorption rate (µmol/g catalyst) at 200 and 300 °C on the Fe-SCR catalyst.

Regarding the isothermal NH_3 desorption (weakly bound ammonia), as seen in Figures 44 and 45, there were clear differences in the rates. The initial desorption rate with 5% water was a much lower than, but this can be explained by the methods used in blank wet experiments. Nonetheless, on the V-SCR-1 the isothermal desorption ended at around

1800 s in dry and at 2500 s with 5% H_2O at 150 °C and it ended on 900 s in and on 2600 s with 5% water at 300 °C. On the Fe-SCR the rate showed a similar trend with and without water at 200 °C and a slight difference at the 300 °C. Rates with and without 5% H_2O at 200 °C showed a similar smooth curve, albeit the rate with 5% water started from around 18 micromoles/g/s while in dry the start was at 20 micromoles/g/s.

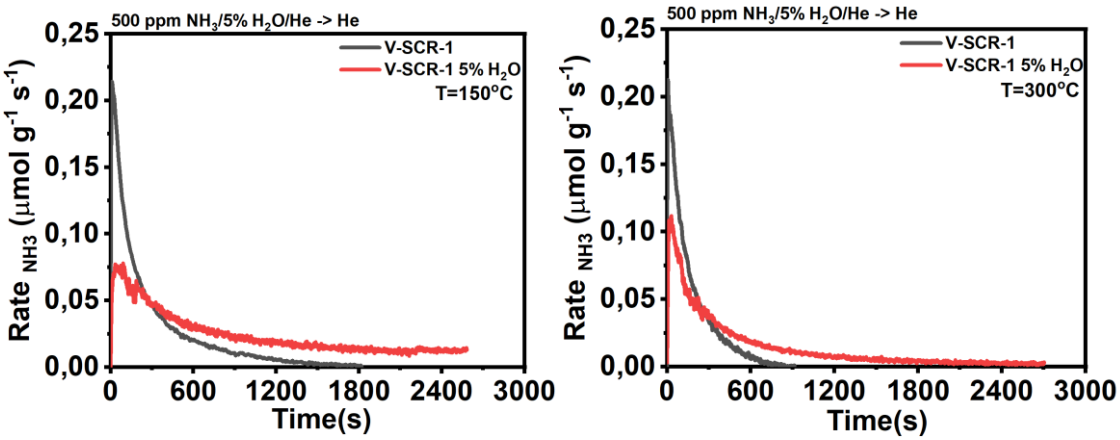


Figure 44. The effect of 5% water on the NH_3 isothermal desorption rate (µmol/g catalyst) on the V-SCR1 catalyst in He flow at 150 and 300 °C.

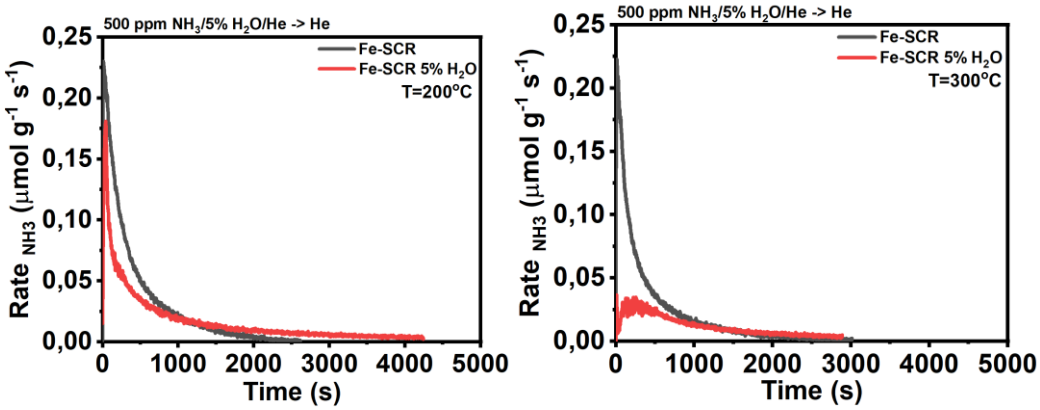


Figure 45. The effect of 5% water on the NH_3 desorption rate (µmol/g catalyst) on the Fe-SCR catalyst in He flow at 150 and 300 °C.

There were some notable differences in TPD results on Fe-SCR and V-SCR-1 catalysts with and without water (Fig. 46 and 47). Regarding the Fe-SCR it seemed that water inhibited the strongly bound ammonia sites, showing significant difference in the peak, in heigh as well as in shape. Instead of having noticeable two peaks in 200 °C and a single pointy peak in 300 °C without water, smaller smoother, curved peaks were detected in the presence of 5% water in both the 200 °C and 300 °C curves. The TPD curve at 150 °C with

water looked to be round as well but encompassing the size of the TPD curve without water. The higher NH_3 response at higher temperatures indicate a higher amount of strongly bound ammonia on the V-SCR1 catalyst surface. Similarly with the Fe-SCR, the shape of the peak is round instead of possessing notable two peaks detected as seen in the flow without water. This might indicate a smoother adsorption desorption across the catalyst in the presence of water instead of having notable adsorption sites. It seemed that no strongly bound ammonia was on the V-SCR1 catalyst surface in wet feed at 300 °C when comparing with the TPD results in dry conditions. According to these experiments, ammonia did not bond strongly on V-SCR catalysts in the presence of water at 300 °C.

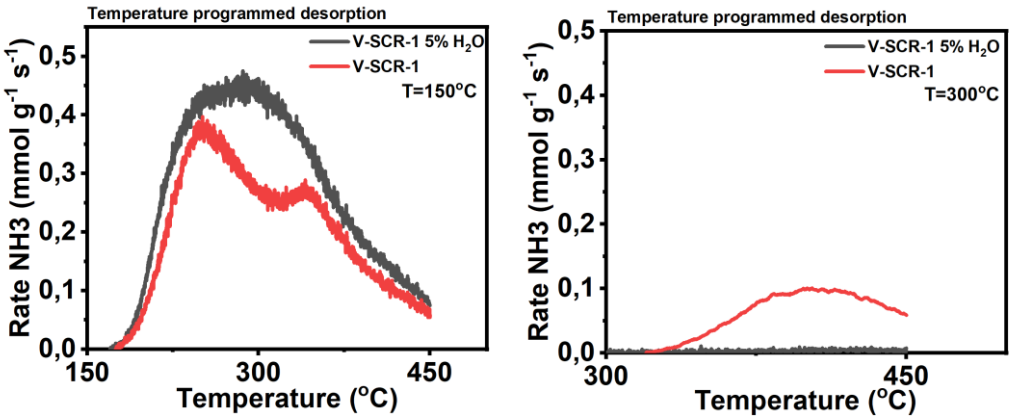


Figure 46. The effect of 5% water on the NH_3 desorption rate (µmol/g catalyst) on the V-SCR1 catalyst during a heating ramp (TPD in He flow)

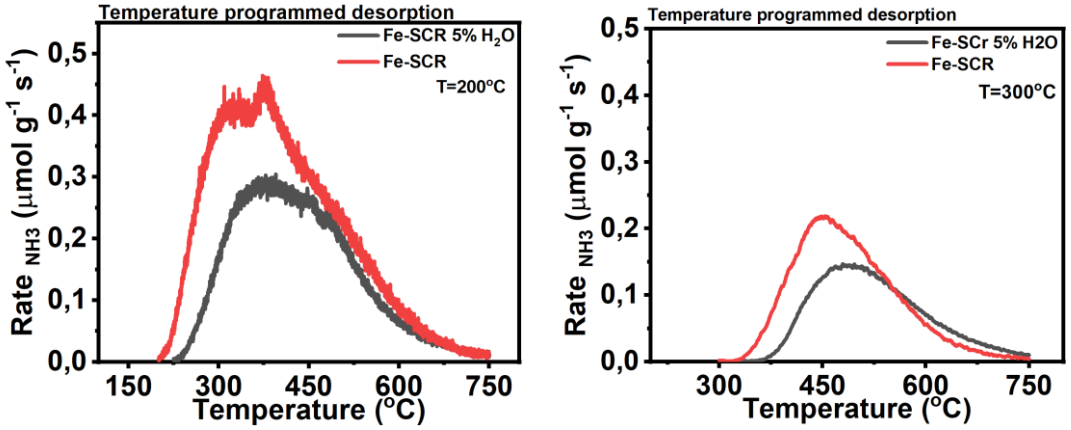


Figure 47. The effect of 5% water on the NH_3 desorption rate (µmol/g catalyst) on the Fe-SCR catalyst during a heating ramp (TPD in He flow)

7 SUMMARY OF RESULTS

Temperature as well as the NH_3 feed concentration of NH_3 had a predominant effect on the adsorption of NH_3 on the SCR catalyst surface. The increase in temperature decreased the amount of ammonia adsorbed on the catalyst surface, which is a trait shared by all catalyst experimented upon, which is a fundamental property related to gas adsorption on solid materials and different SCR catalysts have their specific NH_3 adsorption temperatures in the low temperature range. The Fe-SCR catalyst possessed higher capacity than the V-SCR catalysts. Fe-SCR is known to possess a high adsorption capacity, which agrees with our results.

The NH_3 concentration in the feed also influenced the adsorption capabilities of the SCR catalysts. The lower feed NH_3 concentrations in feed resulted in longer adsorption times, which was expected since it takes more time with lower NH_3 concentrations to saturate the catalyst surface.

Effect of 50 ppm N_2O varied on V-SCR-1 and Fe-SCR catalysts. N_2O had a negligible effect on the NH_3 adsorption capacity on the V-SCR-1 catalyst, which can be attributed to measurement error. Meanwhile on the Fe-SCR catalyst, the effect was more predominant, clearly lowering the adsorption capacity. These differences indicated that N_2O bonds differently on the vanadium catalyst when compared to Fe-beta zeolite catalyst surface.

Water affects the NH_3 adsorption on the Fe-SCR and V-SCR-1 catalysts differently. The presence of water decreased the NH_3 adsorption capacity significantly on the Fe-SCR while on the V-SCR-1 catalyst the adsorption capacity slightly increased at 150 and 300 °C. All NH_3 desorption results (TPD) were summarized to compare the strongly bound NH_3 by catalysts and water effects (Fig. 48). Total NH_3 desorption was much higher on extruded V-SCR-1 than on coated V-SCR-2 due to the higher total catalyst amount. The negligible effect of H_2O on V-SCR-1 and a high effect on Fe-SCR catalyst was seen well in these experiments too. The Fe-SCR catalyst showed the higher NH_3 desorption than the extruded V-SCR-1 catalyst even if it was a coated one with a lower volumetric catalyst amount. This is related to the high specific NH_3 adsorption capacity on Beta zeolite, which is also more sensitive to water inhibition than TiO_2 based V-SCR-1 catalysts.

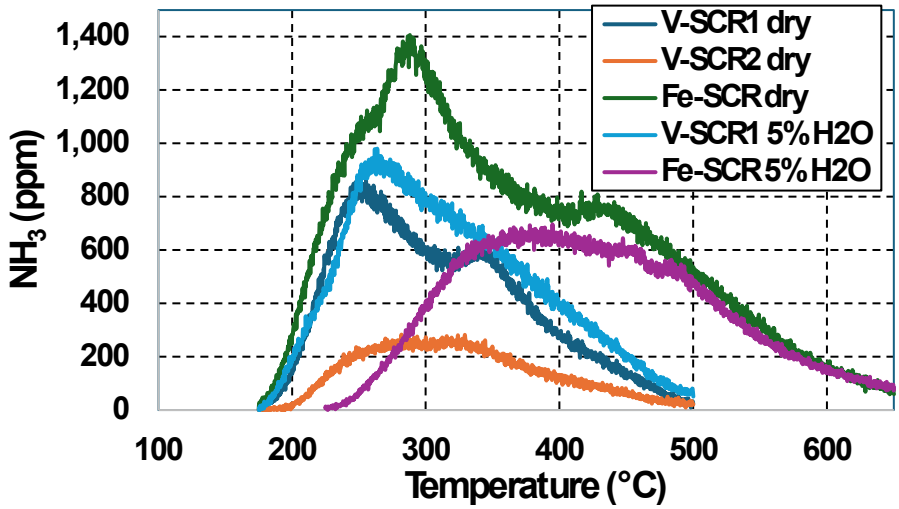


Figure 48. The comparisons of thermal NH_3 desorption (TPD) with the V-SCR and Fe-SCR catalysts in dry and wet conditions.

The Pt-DOC catalyst adsorbed or consumed ammonia most in the ammonia oxidation experiments with pre-adsorbed NH_3 and oxygen. Regarding the isothermal desorption in the presence of oxygen, catalysts performed uniquely. SCR catalysts showed no similar patterns regarding NO, N_2O and N_2 formation but their formation was very low at 300 °C, expect Pt-DOC which is known to oxidize NH_3 to nitrogen oxides and N_2, which is a known property in relation to NH_3 oxidation on ammonia slip catalysts (ASCs).

Possible errors in the experimental values could be attributed to inherent measurement errors in the sample preparation, reaction measurements, MS signal calculations and the effect of water in reactor/sampling lines. Difference values by adsorption and desorption can be evaluated (ads=adsorption, it= isothermal, des= desorption):

$$\text{Difference (ads-des)} = \sum(\text{ads}) - \sum(\text{it-des}) - \sum(\text{des-TPD}) - \sum(\text{blank}) \quad (15)$$

8 CONCLUSIONS

The main point of this master thesis was to determine the effects of varied feed compositions on different SCR catalyst types by utilizing transient kinetic methods equipped by mass spectrometry. In the literature review the SCR catalysts and reactions were reviewed as well as different SCR setups in stationary and mobile and offroad applications. Relevant transient kinetic experimental conditions and results for different catalyst types were reviewed for similarities and differences for the validation of this research.

Experiments gave us a wide variety of data regarding catalyst performance in SCR conditions. Differences in NH_3 adsorption and desorption on the vanadium- and iron-SCR catalysts and transient behaviour was observed in dry and wet conditions. The effect of oxygen and N_2O was investigated in dry conditions. These results confirmed current beliefs about knowledge regarding differences on adsorption NH_3 properties on these SCR catalysts when examined as typical extruded and coated catalyst types. These results allow us to further understand catalysts adsorption and desorption phenomena. The temperature increase had foreknown decreasing effects on the adsorption capacities, meanwhile NH_3 concentration together with the flow rate in the feed means different saturation time of SCR catalysts. The presence of water during NH_3 adsorption conditions had opposite effects results on the V-SCR and Fe-SCR catalysts. 5% water in feed hindered adsorption and decreased NH_3 adsorption capacity on the Fe-SCR catalyst and but correspondingly water increased NH_3 adsorption on the V-SCR catalyst. The NH_3 adsorption capacity at low temperatures has promoting but also requires a careful SCR control design to optimize SCR performance and prevent NH_3 desorption during fast heating phases in use conditions.

Presence of 50 ppm N_2O in feed had no effect on the NH_3 adsorption and desorption capacities on the V-SCR catalyst while there was a major, hindering effect on the adsorption and desorption on the Fe-SCR catalyst. Oxygen in the feed had majorly different effects on the reactions and desorption with pre-adsorbed ammonia on the catalyst surface. In addition to NH_3 desorption, small amounts of NO, NO_2 and N_2 was formed by oxidation reactions, particularly on the Pt-DOC. Understanding the effects of different feed compositions on catalyst functionality is important for furthering future

catalyst development. The experiments conducted at the university of Cyprus gave concrete results in transient behaviour of usual commercial iron and vanadium SCR catalysts in various critical feed compositions.NH_3 adsorption-desorption has a key role to develop SCR catalysts for marine applications using ammonia as a fuel. These observations can be further utilized into developing transient kinetic catalyst models to further develop SCR catalysts.

REFERENCES

Abdul Nasir, J., Guan, J., Keal, T. W., Lu, Y., Sokol, A. A., and Catlow, C. R. A. (2024). The Rôle of Iron in Zeolite Beta for deNO_x Catalysis. Journal of Catalysis, 438, 115696. https://doi.org/10.1016/j.jcat.2024.115696

Appl, M. (2011). Ammonia, 1. Introduction. In: Ullmann's Encyclopedia of Industrial Chemistry. John Wiley and Sons, Ltd. Wiley-VCH Verlag GmbH & Co. KGaA, Weinheim https://doi.org/10.1002/14356007.a02_143.pub3

Appl, M. (2011). Ammonia, 2. Production Processes. In: Ullmann's Encyclopedia of Industrial Chemistry. John Wiley and Sons, Ltd. Wiley-VCH Verlag GmbH & Co. KGaA, Weinheim https://doi.org/10.1002/14356007.o02_o11

Ayodhya, A. S., and Narayanappa, K. G. (2018). An overview of after-treatment systems for diesel engines. Environmental Science and Pollution Research, 25(35), 35034–35047. https://doi.org/10.1007/s11356-018-3487-8

Bardhan, P. (1997). Ceramic honeycomb filters and catalysts. Current Opinion in Solid State and Materials Science, 2(5), 577–583. https://doi.org/10.1016/S1359-0286(97)80048-4

Beale, A. M., Lezcano-Gonzalez, I., Maunula, T., and Palgrave, R. G. (2015). Development and characterization of thermally stable supported V-W-TiO_2 catalysts for mobile NH_3-SCR applications. Catalysis, structure and reactivity, 1(1), 25-34. https://doi.org/10.1179/2055075814Y.0000000005

Carmo, M., Fritz, D. L., Mergel, J., and Stolten, D. (2013). A comprehensive review on PEM water electrolysis. International Journal of Hydrogen Energy, 38(12), 4901–4934. https://doi.org/10.1016/j.ijhydene.2013.01.151

Chen, L., Li, J., and Ge, M. (2011). The poisoning effect of alkali metals doping over nano V_2O_5–WO_3/TiO_2 catalysts on selective catalytic reduction of NO_x by NH_3. Chemical Engineering Journal, 170(2–3), 531–537. https://doi.org/10.1016/j.cej.2010.11.020

Chen, Z., Liu, Q., Liu, H., and Wang, T. (2024). Recent Advances in SCR Systems of Heavy-Duty Diesel Vehicles—Low-Temperature NO_x Reduction Technology and Combination of SCR with Remote OBD. Atmosphere, 15(8), Article 8. https://doi.org/10.3390/atmos15080997

Dąbrowski, A. (2001). Adsorption—From theory to practice. Advances in Colloid and Interface Science, 93(1), 135–224. https://doi.org/10.1016/S0001-8686(00)00082-8

Egerer, J., Grimm, V., Niazmand, K., and Runge, P. (2023). The economics of global green ammonia trade – "Shipping Australian wind and sunshine to Germany." Applied Energy, 334, 120662. https://doi.org/10.1016/j.apenergy.2023.120662

Garg, E., and Zubair, M. (2026). Mass Spectrometer. In StatPearls. StatPearls Publishing. http://www.ncbi.nlm.nih.gov/books/NBK589702/

Grossale, A., Nova, I., and Tronconi, E. (2008). Study of a Fe–zeolite-based system as NH_3-SCR catalyst for diesel exhaust aftertreatment. Catalysis Today, 136(1–2), 18–27. https://doi.org/10.1016/j.cattod.2007.10.117

Guan, B., Zhan, R., Lin, H., and Huang, Z. (2014). Review of state of the art technologies of selective catalytic reduction of NO_x from diesel engine exhaust. Applied Thermal Engineering, 66(1), 395–414. https://doi.org/10.1016/j.applthermaleng.2014.02.021

Gui, R., Zhang, C., Gao, Y., Wang, Q., and Efstathiou, A. M. (2025). Unravelling the multiple effects of H_2O on the NH_3-SCR over Mn2Cu1Al1Ox-LDO by transient kinetics and in situ DRIFTS. Applied Catalysis B: Environment and Energy, 361, 124611. https://doi.org/10.1016/j.apcatb.2024.124611

Heck, R. M., Farrauto, R. J., and Gulati, S. T. (2009). Reduction of NO_x. Catalytic air pollution control: Commercial technology. Hoboken, N.J: John Wiley. https://doi.org/10.1002/9781118397749

Høj, M., Beier, M. J., Grunwaldt, J.-D., and Dahl, S. (2009). The role of monomeric iron during the selective catalytic reduction of NO by NH_3 over Fe-BEA zeolite catalysts. Applied Catalysis B: Environmental, 93(1–2), 166–176. https://doi.org/10.1016/j.apcatb.2009.09.026

Imbihl, R., Scheibe, A., Zeng, Y. F., Günther, S., Kraehnert, R., Kondratenko, V. A., Baerns, M., Offermans, W. K., Jansen, A. P. J., and Santen, R. A. van. (2007). Catalytic ammonia oxidation on platinum: Mechanism and catalyst restructuring at high and low pressure. Physical Chemistry Chemical Physics, 9(27), 3522–3540. https://doi.org/10.1039/B700866J

Katada, N., Igi, H., and Kim, J.-H. (1997). Determination of the Acidic Properties of Zeolite by Theoretical Analysis of Temperature-Programmed Desorption of Ammonia Based on Adsorption Equilibrium. The Journal of Physical Chemistry B, 101(31), 5969–5977. https://doi.org/10.1021/jp9639152

Kleemann, M., Elsener, M., Koebel, M., and Wokaun, A. (2000). Investigation of the ammonia adsorption on monolithic SCR catalysts by transient response analysis. Applied Catalysis B: Environmental, 27(4), 231–242. https://doi.org/10.1016/S0926-3373(00)00158-2

Králik, M. (2014). Adsorption, chemisorption, and catalysis. Chemical papers, 68(12), 1625-1638. https://doi.org/10.2478/s11696-014-0624-9

Lai, J.-K., and Wachs, I. E. (2018). A Perspective on the Selective Catalytic Reduction (SCR) of NO with NH_3 by Supported V_2O_5–WO_3/TiO_2 Catalysts. ACS Catalysis, 8(7), 6537–6551. https://doi.org/10.1021/acscatal.8b01357

Lehtoranta, K., Vesala, H., Koponen, P., and Korhonen, S. (2015). Selective Catalytic Reduction Operation with Heavy Fuel Oil: NO_x, NH_3, and Particle Emissions. Environmental Science and Technology, 49(7), 4735–4741. https://doi.org/10.1021/es506185x

Li, S., Cheng, G., Chen, H., Li, R., Xia, P., Li, Y., Liang, X., and Wang, K. (2025). Mechanism of N_2O formation in catalytic after-treatment systems of ammonia/hydrogen-

fuelled engines. Physical Chemistry Chemical Physics, 27(25), 13382–13389. https://doi.org/10.1039/D4CP02075H

Lisi and Cimino, 2020, L., and Cimino, S. (2020). Poisoning of SCR Catalysts by Alkali and Alkaline Earth Metals. Catalysts, 10(12), 1475. https://doi.org/10.3390/catal10121475

Liu, K., Yan, Z., He, H., Feng, Q., and Shan, W. (2019). The effects of H_2O on a vanadium-based catalyst for NH3-SCR at low temperatures: A quantitative study of the reaction pathway and active sites. Catalysis Science and Technology, 9(20), 5593–5604. https://doi.org/10.1039/C9CY01370A

Liu, Q., Bian, C., Ming, S., Guo, L., Zhang, S., Pang, L., Liu, P., Chen, Z., and Li, T. (2020). The opportunities and challenges of iron-zeolite as NH_3-SCR catalyst in purification of vehicle exhaust. Applied Catalysis A: General, 607, 117865. https://doi.org/10.1016/j.apcata.2020.117865

Lu, X., Geng, P., and Chen, Y. (2020). NO_x Emission Reduction Technology for Marine Engine Based on Tier-III: A Review. Journal of Thermal Science, 29(5), 1242–1268. https://doi.org/10.1007/s11630-020-1342-y

Martín, N., Vennestrøm, P. N. R., Thøgersen, J. R., Moliner, M., and Corma, A. (2017). Fe-Containing Zeolites for NH_3-SCR of NO_x: Effect of Structure, Synthesis Procedure, and Chemical Composition on Catalytic Performance and Stability. Chemistry - A European Journal, 23(54), 13404–13414. (125370492). https://doi.org/10.1002/chem.201701742

Maunula, T., (2013). NO_x Reduction with the Combinations on LNT and SCR in Diesel Applications,"SAE Int. J. Mater. Manf. 7(1), doi:10.4271/2013-24-0161.

Maunula, T., Savimäki, A., Viitanen, A., Kinnunen, T., and Kanniainen, K. (2013), Thermally durable vanadium-SCR catalysts for diesel applications, SAE Paper 2013-01-0796.

Maunula, T. and Wolff, T., (2016) Durable copper and iron SCR catalysts for mobile diesel applications, SAE Paper 2016-01-2214.

Maunula, T., Tuikka, M., and Wolff, T. (2020). The Reactions and Role of Ammonia Slip Catalysts in Modern Urea-SCR Systems. Emission Control Science and Technology, 6(4), 390–401. https://doi.org/10.1007/s40825-020-00171-1

Metkar, P. S., Harold, M. P., and Balakotaiah, V. (2012). Selective catalytic reduction of NO_x on combined Fe- and Cu-zeolite monolithic catalysts: Sequential and dual layer configurations. Applied Catalysis B: Environmental, 111–112, 67–80. https://doi.org/10.1016/j.apcatb.2011.09.019

Miller, B. G. (2017). Clean coal engineering technology (Second edition.). Butterworth-Heinemann.

Nova, I., Tronconi, E., and Tronconi, E. (2014). Urea-SCR Technology for deNOx After Treatment of Diesel Exhausts. New York, NY: Springer Nature. https://doi.org/10.1007/978-1-4899-8071-7

Reiter, A. J., and Kong, S.-C. (2011). Combustion and emissions characteristics of compression-ignition engine using dual ammonia-diesel fuel. Fuel, 90(1), 87–97. https://doi.org/10.1016/j.fuel.2010.07.055

Scheibe, A., Hinz, M., and Imbihl, R. (2005). Kinetics of ammonia oxidation on stepped platinum surfaces: II. Simulation results. Surface Science, 576(1), 131–144. https://doi.org/10.1016/j.susc.2004.12.007

Scheuer, A., Votsmeier, M., Schuler, A., Gieshoff, J., Drochner, A., and Vogel, H. (2009). NH_3-Slip Catalysts: Experiments Versus Mechanistic Modelling. Topics in Catalysis, 52(13), 1847–1851. https://doi.org/10.1007/s11244-009-9351-9

Shan, Y., Du, J., Zhang, Y., Shan, W., Shi, X., Yu, Y., Zhang, R., Meng, X., Xiao, F.-S., and He, H. (2021). Selective catalytic reduction of NO_x with NH_3: Opportunities and challenges of Cu-based small-pore zeolites. National Science Review, 8(10), nwab010. https://doi.org/10.1093/nsr/nwab010

Shi, J., Zhang, Y., Zhang, Z., Fan, Z., Chen, M., Zhang, Z., and Shangguan, W. (2018). Water promotion mechanism on the NH_3-SCR over Fe-BEA catalyst. Catalysis Communications, 115, 59–63. https://doi.org/10.1016/j.catcom.2018.07.012

Shwan, S., Jansson, J., Korsgren, J., Olsson, L., and Skoglundh, M. (2012). Kinetic modeling of H-BEA and Fe-BEA as NH3-SCR catalysts—Effect of hydrothermal treatment. Catalysis Today, Special Issue Dedicated to Professor Pio Forzatti on the Occasion of His 65th Birthday, 197(1), 24–37. https://doi.org/10.1016/j.cattod.2012.06.014

Smart, K. (2022). Review of Recent Progress in Green Ammonia Synthesis: Decarbonisation of fertiliser and fuels via green synthesis. Johnson Matthey Technology Review, 66(3), 230–244. https://doi.org/10.1595/205651322x16334238659301

Sun, Q., Wang, N., and Yu, J. (2021). Advances in Catalytic Applications of Zeolite-Supported Metal Catalysts. Advanced Materials, 33(51), 2104442. https://doi.org/10.1002/adma.202104442

Szymaszek, A., Samojeden, B., and Motak, M. (2020). The Deactivation of Industrial SCR Catalysts—A Short Review. Energies, 13(15), 3870. https://doi.org/10.3390/en13153870

Urban, P. L. (2016). Quantitative mass spectrometry: An overview. Philosophical Transactions of the Royal Society A: Mathematical, Physical and Engineering Sciences, 374(2079), 20150382. https://doi.org/10.1098/rsta.2015.0382

Wu, Y., Zhou, X., Zhou, J., Hu, Z., Cai, Q., and Lu, Q. (2023). A comprehensive review of the heavy metal issues regarding commercial vanadium-titanium-based SCR catalyst. Science of The Total Environment, 857, 159712. https://doi.org/10.1016/j.scitotenv.2022.159712

Yao, H., Chen, Y., Wei, Y., Zhao, Z., Liu, Z., and Xu, C. (2012). A periodic DFT study of ammonia adsorption on the V_2O_5 (001), V_2O_5 (010) and V_2O_5 (100) surfaces: Lewis versus Brönsted acid sites. Surface Science, 606(21), 1739–1748. https://doi.org/10.1016/j.susc.2012.07.020

Ye, B., Jeong, B., Lee, M., Kim, T. H., Park, S.-S., Jung, J., Lee, S., & Kim, H.-D. (2022). Recent trends in vanadium-based SCR catalysts for NOx reduction in industrial applications: Stationary sources. Nano Convergence, 9(1), 51. https://doi.org/10.1186/s40580-022-00341-7

Zannis, T. C., Katsanis, J. S., Christopoulos, G. P., Yfantis, E. A., Papagiannakis, R. G., Pariotis, E. G., Rakopoulos, D. C., Rakopoulos, C. D., and Vallis, A. G. (2022). Marine Exhaust Gas Treatment Systems for Compliance with the IMO 2020 Global Sulfur Cap and Tier III NO_x Limits: A Review. Energies, 15(10), 3638. https://doi.org/10.3390/en15103638

Zhang, T., Liu, Z., Liu, J., Jiang, M., Xia, X., Shan, X., Shan, Y., Shi, X., Yu, Y., and He, H. (2026). Increased NH3-SCR activity and stability of Fe-Beta catalysts achieved by using Al-rich zeolite. Journal of Environmental Sciences, 159, 809–818. https://doi.org/10.1016/j.jes.2025.03.036

Zhu, M., Lai, J.-K., Tumuluri, U., Ford, M. E., Wu, Z., and Wachs, I. E. (2017). Reaction Pathways and Kinetics for Selective Catalytic Reduction (SCR) of Acidic NO_x Emissions from Power Plants with NH_3. ACS Catalysis, 7(12), 8358–8361. https://doi.org/10.1021/acscatal.7b03149

Zhu, Y., Xia, C., Shreka, M., Wang, Z., Yuan, L., Zhou, S., Feng, Y., Hou, Q., and Ahmed, S. A. (2020). Combustion and emission characteristics for a marine low-speed diesel engine with high-pressure SCR system. Environmental Science and Pollution Research, 27(12), 12851–12865. https://doi.org/10.1007/s11356-019-04194-2